

The dependence of luminous efficiency on chromatic adaptation

Andrew Stockman

Institute of Ophthalmology, University College London,
London, UK



Herbert Jägle

Centre for Ophthalmology, Eberhard Karls University,
Tübingen, Germany



Markus Pirzer

Centre for Ophthalmology, Eberhard Karls University,
Tübingen, Germany



Lindsay T. Sharpe

Institute of Ophthalmology, University College London,
London, UK



We investigated the dependence of luminous efficiency on background chromaticity by measuring 25-Hz heterochromatic flicker photometry (HFP) matches in six genotyped male observers on 21 different 1000-photopic-troland adapting fields: 14 spectral ones ranging from 430 to 670 nm and 7 bichromatic mixtures of 478 and 577 nm that varied in luminance ratio. Each function was analyzed in terms of the best-fitting linear combination of the long- (L) and middle- (M) wavelength sensitive cone fundamentals of A. Stockman and L. T. Sharpe (2000). Taking into account the adapting effects of both the backgrounds and the targets, we found that luminous efficiency between 603 and 535 nm could be predicted by a simple model in which the relative L- and M-cone weights are inversely proportional to the mean cone excitations produced in each cone type multiplied by a single factor, which was roughly independent of background wavelength (and may reflect relative L:M cone numerosity). On backgrounds shorter than 535 nm and longer than 603 nm, the M-cone contribution to luminous efficiency falls short of the proportionality prediction but most likely for different reasons in the two spectral regions.

Keywords: luminance, chromatic adaptation, cone fundamentals, heterochromatic flicker photometry (HFP), luminous efficiency, minimum flicker

Citation: Stockman, A., Jägle, H., Pirzer, M., & Sharpe, L. T. (2008). The dependence of luminous efficiency on chromatic adaptation. *Journal of Vision*, 8(16):1, 1–26, <http://journalofvision.org/8/16/1/>, doi:10.1167/8.16.1.

Introduction

Spectral luminous efficiency functions are relative weighting functions that are used to convert physical or radiometric measures, such as radiance, to visually relevant or photometric ones, such as luminance. They define the relative visual “effectiveness” of lights of different wavelength. In 1924, the CIE established a luminous efficiency function, $V(\lambda)$, for photopic (cone) vision, which has since become the standard for business and industry. In visual science, $V(\lambda)$ or its variants has been assumed to correspond to the spectral sensitivity of a hypothetical human postreceptor channel, the so-called “luminance” channel with additive inputs from the long-wavelength sensitive (L-) and middle-wavelength sensitive (M-) cones (e.g., Smith & Pokorny, 1975). The widespread acceptance of these functions, however, downplays the many difficulties inherent in their derivation and application (see, for discussion Sharpe, Stockman, Jagla, & Jägle, 2005).

In an attempt to overcome some of these difficulties, we recently determined a luminous efficiency function for 2°

photopic viewing conditions, which we called $V^*(\lambda)$, based exclusively on HFP measurements made in 40 genotyped observers (Sharpe et al., 2005). The function was obtained under neutral adaptation that corresponded to daylight D_{65} adaptation and is defined as a linear combination of the Stockman and Sharpe (2000) L- and M- cone fundamentals. The specification of a fixed luminous efficiency function for neutral adaptation, and its definition in terms of standardized L- and M-cone spectral sensitivities, is important for practical photometry and for modeling visual performance under neutral or achromatic conditions. In terms of modeling performance under “real world” conditions, however, it is a gross oversimplification. Photopic luminous efficiency functions are not fixed in spectral sensitivity but change with chromatic adaptation (e.g., De Vries, 1948b; Eisner, 1982; Eisner & MacLeod, 1981; Ikeda & Urakubo, 1968; King-Smith & Webb, 1974; Marks & Bornstein, 1973; Stockman, MacLeod, & Vivien, 1993; Stromeyer, Chaparro, Toliás, & Kronauer, 1997; Stromeyer, Cole, & Kronauer, 1987; Swanson, 1993). Thus, any luminous efficiency function strictly applies only to the limited

conditions of chromatic adaptation under which it was measured. Luminous efficiency is therefore quite distinct from color matching functions (CMFs) or cone fundamentals, which do not change in spectral sensitivity (unless the photopigment is bleached at high intensity levels). Consequently, the correspondence between luminous efficiency and the CIE $\bar{y}(\lambda)$ CMF is largely a contrivance: the former *should* change with chromatic adaptation, but the latter does not.

Defining a photopic luminous efficiency measure that can be generalized to changes in both background luminance and background chromaticity is a daunting proposition. Here, we focus merely on describing the effects of changing background chromaticity. Twenty-one backgrounds, each of 3 log photopic trolands were used: 14 spectral ones ranging in wavelength from 430 to 670 nm and 7 bichromatic mixtures comprising 478 and 577 nm fields in different luminance ratios. Each HFP spectral sensitivity curve was analyzed as a linear combination of the Stockman and Sharpe (2000) L- and M-cone fundamentals. Our aim was to understand and model how the relative contributions of the L- and M-cones to HFP depend upon background chromaticity. The analysis was complicated by the fact that the mean state of adaptation depended not only on the fixed luminance of the background but also on the luminances of the flickering reference and variable-wavelength test lights. Nonetheless, a relatively simple predictive model was developed. The extent to which this model can be applied to luminance levels other than 3 log trolands is fundamentally limited, but it should at least be *approximately* correct for conditions under which Weber's Law applies independently for each cone signal (see [Discussion](#) section).

To monitor the effects of chromatic adaptation on luminous efficiency, we measured the efficiency of targets superimposed on various adapting backgrounds. Consequently, our luminance measure is an incremental one and, thus, only partially related to the absolute luminances of the adapting backgrounds themselves.

Methods

Subjects

Six male observers with normal visual acuity served as subjects in this study. All had normal trichromatic color vision as defined by standard tests, including their Rayleigh match on a Nagel Type I anomaloscope. They were genotyped according to the alanine/serine (ala¹⁸⁰/ser¹⁸⁰) photopigment polymorphism at amino-acid position 180 in the L-cone photopigment gene: S1, S2, S3, and S4 have L(ser¹⁸⁰), while A1 and A2 have L(ala¹⁸⁰). Their ages ranged between 18 and 53 years.

Genotyping

The classification of photopigment genes is complicated by polymorphisms in the normal population, the most common of which is the frequent replacement of serine by alanine at codon 180 in exon 3 of the X-chromosome-linked opsin gene. Approximately 56% of a large sample of 304 Caucasian males with normal and deutan color vision have the serine variant [identified as L(ser¹⁸⁰)] and 44% the alanine variant [identified as L(ala¹⁸⁰)] for their L-cone gene (summarized in Table 1 of Stockman & Sharpe, 2000). In contrast, in the M-cone pigment, the ala¹⁸⁰/ser¹⁸⁰ polymorphism is much less frequent, 93%–94% of males having the ala¹⁸⁰ variant (Neitz & Neitz, 1998; Winderickx, Battisti, Hibiya, Motulsky, & Deeb, 1993). Therefore, we only identified the genotype with respect to the ser¹⁸⁰/ala¹⁸⁰ polymorphism in the first (L-cone) photopigment gene in the array of our observers. Given that we used 6 subjects, there is about a 33% chance that one of them will have the ser¹⁸⁰ M-cone variant. This variant would cause a modest red shift in the luminous efficiency function and a corresponding increase in the estimated L-cone weight. The genotype was first determined by amplification, using total genomic DNA, of exon 3 followed by digestion with Fnu4H as previously described (Deeb, Hayashi, Winderickx, & Yamaguchi, 2000).

Apparatus

Details of the design and calibration of the four-channel Maxwellian-view optical system, used to measure the HFP sensitivities, are provided elsewhere (Sharpe, Stockman, Jägle et al., 1998; Sharpe et al., 2005). Briefly, all four of the optical channels originated from a 75-W xenon arc lamp run at constant current. In addition, the beam path in one of the channels (Channel 4) could be interrupted by the placement of a half-silvered mirror, allowing the source of illumination to be replaced by a 12-V, 50-W tungsten halogen lamp.

Two of the channels (Channels 1 and 2) provided the 2° (diameter) flickering test and reference lights, which were alternated at 25 Hz in opposite-phase square wave. A frequency of 25 Hz was chosen to obviate signals from the rods and S-cone pathways and because it was the same as that used to measure the flicker data guiding the derivation of the Stockman and Sharpe (2000) L- and M-cone fundamentals (see [Advantages of using 25-Hz flicker](#) section). Wavelengths were selected by grating monochromators (Model CM110, CVI Spectral Products, Putnam, USA), with 0.6-mm entrance and exit slits, which generated triangular spectral profiles having a full bandwidth at half-maximum (FWHM) of <5 nm. The wavelength of the reference light was always set to 560 nm, whereas that of the test light was varied from 420 to 680 nm

in 20-nm steps. At wavelengths longer than 560 nm, a glass cut-off filter (Schott OG550, Mainz, Germany), which blocked short wavelengths but transmitted wavelengths higher than 550 nm, was inserted after the exit slit of both monochromators.

The other two channels (Channels 3 and 4) provided the 16° diameter neutral and chromatic adapting fields. Channel 3 provided chromatic adapting fields by means of a grating monochromator, the properties of which were identical to those of the monochromators in Channels 1 and 2. The wavelength was set at either 430, 444, 463, 495, 517, 535, 549, 563, 577, 589, 603, 619, 645, or 670 nm. The retinal illuminance of the background adapting field was held constant at 3.0 log photopic td, regardless of wavelength.

Channel 4 provided the second chromatic adapting field of 478 nm in the bichromatic mixture experiments. The beam was rendered nearly monochromatic by inserting an interference filter (Schott, Mainz, Germany), with a full bandwidth at half-amplitude of 8 nm in the path of the 75-W xenon arc lamp.

Infrared radiation was eliminated by heat-absorbing glass (Schott, Mainz, Germany) placed early in each beam. The images of the arcs or filament were less than 1.5 mm in diameter at the plane of the observer's pupil. Circular field stops placed in collimated portions of each beam at the focal length of the final Maxwellian lens defined the test/reference lights and adapting fields as seen by the observer. Mechanical shutters driven by a computer-controlled square-wave generator were positioned in each channel near focal points of the xenon arc. The optical waveforms so produced were monitored periodically with a Pin-10 diode (United Detector Technology, Santa Monica, CA) and oscilloscope. Fine control over the luminance of the stimuli was achieved by variable 2.0-log unit linear (LINOS Photonics, formerly, Spindler and Hoyer) or 4.0-log unit circular (Rolyn Optics, Covina, California, USA) neutral density wedges positioned at focal points of the arc lamps or filaments and by insertion of fixed neutral density filters in parallel portions of the beams. The position of the observer's head was maintained by a rigidly mounted dental wax impression.

Procedure

Corneal spectral sensitivities were measured by HFP within the central 2° of the fovea. The reference light of 560 nm was alternated at a rate of 25 Hz, in opposite phase with a superimposed test light of one of the 14 test wavelengths. Both flickering stimuli were superimposed on a 16° diameter adapting field with a retinal illuminance of 3.0 log trolands. The HFP task was easily explained to the subjects who were experienced and well trained. None expressed any difficulties with the technique, except on long-wavelength fields (in particular, 645 and 670 nm) on

which the phase differences between the L- and M-cone signals are large (see [Complexities](#) section). Our reasons for choosing this variant of the HFP task are fully discussed in our previous paper (Sharpe et al., 2005).

At the start of the measurement of a spectral sensitivity curve, the radiance of the 560-nm reference flickering light (presented alone on the background without the test light) was adjusted by the subject to be at the threshold for just detecting flicker. Five adjustments were made and averaged. The reference was then fixed at 0.2 log unit above this value for the HFP measurements. The test light was next added to the reference light in counterphase. The subject adjusted the intensity of the test light until the flicker percept produced by the combined test and reference lights disappeared or was minimized. Each setting was repeated three times; after each setting, the intensity of the flickering test light was randomly reset to a higher or lower intensity so that the subject had to readjust the intensity to find the best setting. The test wavelength was varied randomly in 20-nm steps from 420 to 680 nm, and each wavelength was presented 4 separate times, within a single run. As noted below, between one and six complete runs were performed by each subject for each of the 23 different adapting field conditions.

The adapting conditions were the 14 spectral backgrounds ranging in wavelength from 430 to 670 nm and the 7 bichromatic mixtures of 478- and 577-nm adapting fields. The luminance of all fields whether single or combined was 3 log photopic trolands. The bichromatic mixtures were: (100%) 478 nm + (0%) 577 nm, (75%) 478 nm + (25%) 577 nm, (62.5%) 478 nm + (37.5%) 577 nm, (50%) 478 nm + (50%) 577 nm, (37.5%) 478 nm + (62.5%) 577 nm, (25%) 478 nm + (75%) 577 nm, and (0%) 478 nm + (100%) 577 nm.

Calibration

During the experiments, the quantal flux densities of the test/reference lights and adapting fields were measured *in situ* at the plane of the observer's pupil with a silicon photodiode (Model SS0-PD50-6-BNC, Gigahertz-Optics, München, Germany), which was calibrated against the German National Standard and a picoammeter (Model 486, Keithley, Germering, Germany). The fixed and variable neutral density filters were calibrated *in situ* for all test and field wavelengths. Particular care was taken in calibrating the monochromators and interference filters: a spectroradiometer (Compact Array Spectrometer CAS-140, Instrument Systems, München, Germany), with a spectral resolution better than 0.2 nm, was used to measure the center wavelength and the bandpass (full-width at half-maximum, FWHM) at each wavelength. The absolute wavelength accuracy was better than 0.2 nm, whereas the resolution of the wavelength settings was better than 0.15 nm (Sharpe, Stockman, Jägle et al., 1998).

The wavelengths of the two CVI monochromators were additionally calibrated against a low-pressure mercury source (Model 6035, L.O.T.-Oriel, Darmstadt, Germany).

Each adapting field or field mixture was set to be 3 log td. The mean luminance level of the adapting field plus the near-threshold 25-Hz reference and target lights, however, was slightly higher, being on average approximately 3.2 log td.

Curve fitting

All curve-fitting was carried out with the standard Marquardt–Levenberg algorithm implemented in Sigma-Plot (SPSS, Chicago), which was used to find the coefficients (parameters) of the independent variable or variables that gave the “best least squares fit” between our model and the data. This algorithm seeks the values of the parameters that minimize the sum of the squared differences between the values of the observed and predicted values of the dependent variable or variables. Fits were made to logarithmic quantal spectral sensitivity data.

Nomenclature

We call the luminous efficiency for incremental lights on a background: $V_{\mu}^*(\lambda)$. The symbol μ in this context refers to the background chromaticity (which can be defined in the model as the monochromatic wavelength that produces the same ratio of M:L-cone excitations as the actual background). The previously published $V^*(\lambda)$ function (Sharpe et al., 2005) is a special case of $V_{\mu}^*(\lambda)$, which we now refer to as $V_{D65}^*(\lambda)$.

Advantages of using 25-Hz flicker

There are several advantages of using 25-Hz flicker. First, it eliminates the contributions of chromatically opponent color channels, which can disturb flicker null settings at lower temporal frequencies. Second, it minimizes sluggish spectrally opponent (but achromatic) L- and M-cone contributions that can be prominent in HFP at lower frequencies on some spectral fields. These interactions may be especially problematical near 15 Hz, where large frequency- and intensity-dependent changes in flicker sensitivity and phase delay are found, but they decrease as the frequency is further increased (see, e.g., Stockman, Montag, & MacLeod, 1991; Stockman & Plummer, 1994, 2005b; Stockman, Plummer, & Montag, 2005; Stromeyer et al., 1997, 2000; Swanson, Pokorny, & Smith, 1987). Third, it minimizes the small contributions to HFP from the S-cones, which are found on longer wavelength fields (e.g., Stockman, MacLeod, &

DePriest, 1991). Fourth, it minimizes any flicker contributions from the rods (e.g., Conner & MacLeod, 1977; Sharpe, Stockman, & MacLeod, 1989), which may not be fully saturated by 3 log photopic troland long-wavelength fields.

It should be noted that the choice of task for measuring luminous efficiency is complicated by often competing requirements. The first and arguably most important requirement is to yield an additive, practicable measure of luminous efficiency, according to which the photometry of narrow-band and broad-band lights is consistent (see above). The second is to yield a measure that corresponds in some meaningful way to the visual effectiveness of lights in the real world. The third, which is perhaps more relevant to the needs of visual science, is that the task should depend on the so-called luminance channel, which is more sensitive to high-frequency flicker than the chromatic channels (see, e.g., Lennie, Pokorny, & Smith, 1993). The choice is inevitably a compromise. The use of 25-Hz HFP favors the first and third requirements.

Results

Flicker photometric spectral sensitivity data

Figure 1 shows flicker photometric spectral sensitivity data for subject S1 plotted as a function of the wavelength of the test target. The top panel presents HFP data measured on spectral backgrounds from 430 to 670 nm, and the bottom panel presents data measured on bichromatic field mixtures from 100% 478 nm (100/0) to 100% 577 nm (0/100). As the field wavelength increases, or the bichromatic mixture becomes more yellow, there is a relative loss of sensitivity to long-wavelength targets and an increase in sensitivity to short-wavelength targets. These effects can be seen more clearly in Figure 2, in which the HFP data have been normalized at a target wavelength of 560 nm. The top panel of Figure 2 shows the data obtained on spectral backgrounds (the solid and dashed lines join the 462- and 645-nm field data, respectively), and the lower panel shows the data obtained on bichromatic mixtures [the solid and dashed lines join the 100/0 (blue field) and 0/100 (yellow field) data, respectively]. As expected, chromatic adapting fields change the shape of the luminous efficiency function. Longer wavelength (or more yellow) fields decrease long-wavelength sensitivity relative to short, which is consistent with a relative reduction in the L-cone contribution to HFP. In contrast, shorter wavelength (or more blue) fields increase long-wavelength sensitivity relative to short, which is consistent with a relative reduction in the M-cone contribution.

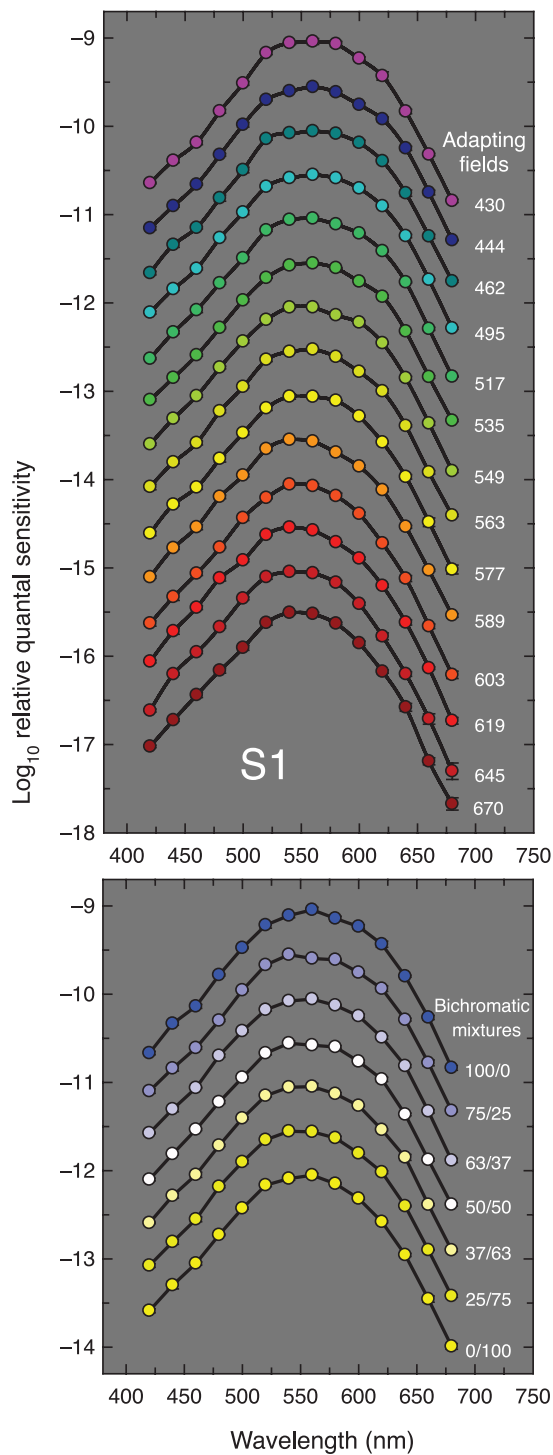


Figure 1. Luminous efficiency (HFP matches) versus target wavelength for observer S1. The upper panel displays his HFP thresholds determined on the 14 spectral adapting fields, which are identified by their wavelength in nanometers. The thresholds are color-coded according to the approximate appearance of the adapting fields. The lower panel displays his HFP thresholds determined on the 7 bichromatic, 478 + 577 nm, adapting fields that varied in luminance ratio, which are also color-coded according to the approximate appearance of the mixtures. 100/0 refers to 100% blue and 0% yellow in the mixture, 75/25 to 75% blue and 25% yellow, and so on.

Our goal is to model these changes in spectral sensitivity in terms of changes in the relative M- and L-cone contributions to HFP. First, we consider two complexities that affect the analysis.

Complexities

The effects of background luminance

Below bleaching levels, the principal mechanism of steady-state cone light adaptation is the speeding up of the visual response and the concomitant shortening of the

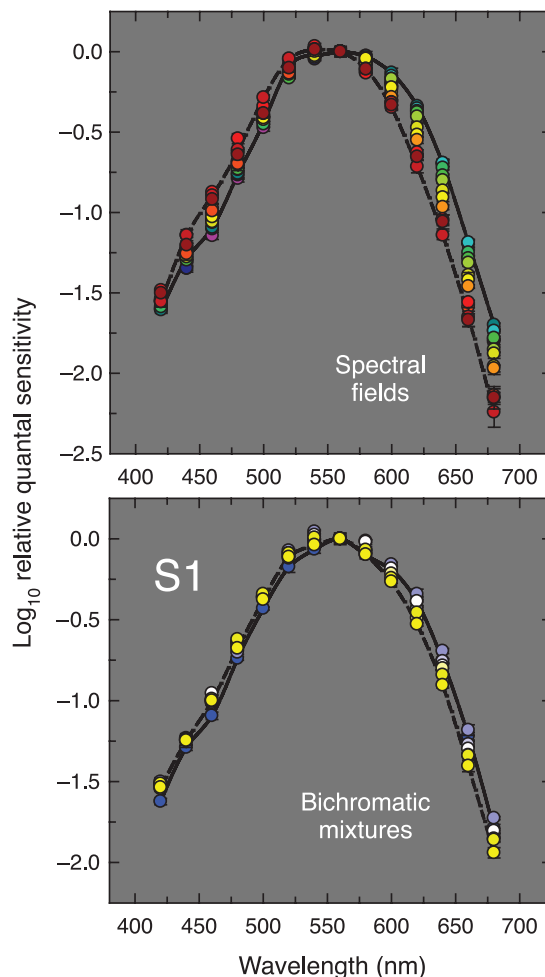


Figure 2. Luminous efficiency (HFP matches) versus target wavelength for observer S1, as shown in Figure 1, but normalized at 560 nm. The upper panel displays the HFP thresholds determined on the 14 spectral adapting fields. The solid line is drawn through the data obtained on the 462-nm field, and the dashed line is drawn through the data obtained on the 645-nm field. The lower panel displays his HFP thresholds determined on the 7 bichromatic, 478 + 577 nm, adapting fields that varied in luminance ratio. The solid line is drawn through the data obtained on the 478-nm field alone (100/0), and the dashed line is drawn through the data obtained on the 577-nm field alone (0/100). Symbols as Figure 1.

visual integration time, so that although observers become more insensitive as the light level rises, they also become relatively more sensitive to flicker of higher temporal frequencies (e.g., De Lange, 1958, 1961; Green, 1968; Kelly, 1961, 1974; MacLeod, 1978; Matin, 1968; Sperling & Sondhi, 1968; Stockman, Langendörfer, Smithson, & Sharpe, 2006; Tranchina, Gordon, & Shapley, 1984; Watson, 1986). As a result, the sensitivity to 25-Hz flicker declines at lower adaptation levels more slowly with background intensity than the sensitivity to lower frequencies. Weber's Law is reached for 25-Hz flicker on neutral or middle-wavelength backgrounds of about 3 log td for achromatic flicker (e.g., De Lange, 1958) and for M-cone flicker (Stockman, Langendörfer et al., 2006) and holds at luminances greater than 3 log td. Above 3 log td (or for spectral fields above a field radiance that has an equivalent effect on the M- and L-cones as a 3 log td neutral or middle-wavelength field), therefore, the temporal properties of the M- and L-cones at 25 Hz—at least in terms of their modulation sensitivities and phase delays—are roughly asymptotic and thus relatively immune to changes in background luminance (Stockman, Langendörfer et al., 2006). However, if the adaptive state of one of the two cone types falls below those asymptotic levels, then its relative contribution to 25-Hz HFP function will fall, and its signals will be delayed (see below). Such a fall occurs for the M-cones on long-wavelength fields of 3 log trolands (see red symbols, Figure 5, below) owing to the relative insensitivity of the M-cones to longer wavelengths. To avoid such difficulties, we have confined our main analysis to background chromaticities on which we estimate that both cone types have reached Weber's Law for 25-Hz flicker detection.

We can determine which fields should be excluded from our analysis from the relative M- and L-cone excitations produced by each background (Stockman & Sharpe, 2000). Data obtained on fields of 589 nm or shorter can be retained, because the M-cones are always sufficiently light adapted [relative to equal peak quantal sensitivities, they are between 0.28 log unit less sensitive (at 589 nm) and 0.23 log unit more sensitive (at 462 nm) to the fields than the L-cones]. However, on longer wavelength fields, the differences in M- and L-cone excitation can be substantial. On 3 log troland fields of 619, 645, and 670 nm, to which the M-cones are 0.68, 1.01, and 1.18 log units, respectively, less sensitive than the L-cones, the M-cone contribution to 25-Hz HFP will drop because of low M-cone adaptation levels (see Stockman, Langendörfer et al., 2006)—as indeed we find (see Figure 5, below). On the 603-nm field, on which the M-cones are 0.46 log unit less sensitive than the L-cones, the expectations are less clear. Since the data at 603 nm are consistent with a Weber's Law model (see below), we have retained them in our analysis. The M-cone adaptation data on which these predictions are based were obtained in two protanopes and so should be relatively unaffected by second-site cone-opponent suppression (see Stockman, Langendörfer et al., 2006).

The problem of the M-cones being relatively unadapted on long-wavelength fields is compounded by potentially large phase delays between the M- and L-cone signals. From our recent model and data (Stockman, Langendörfer et al., 2006), we estimate that the M-cone signals will be phase delayed by approximately 103° at 670 nm, 95° at 645 nm, and 52° at 619 nm relative to the L-cone signals. By simple vector analysis (e.g., Equation 4 of Stockman et al., 2005) and assuming M- and L-cone signals of equal amplitude (the most extreme case for cancellation), we estimate that the resultant amplitude of the combined M- and L-cone signals would be reduced by 0.21 log unit at 670 nm, 0.17 at 645 nm, and 0.05 at 619 nm. Indeed, the phase differences at 670 nm are large enough to make the additive luminance channel weakly opponent at 25 Hz (see Drum, 1977). However, phase differences between the L- and M-cone signals at 603 nm and lower wavelengths can be safely ignored because they are no more than 17° and, therefore, will reduce the amplitude by less than 0.02 log unit.

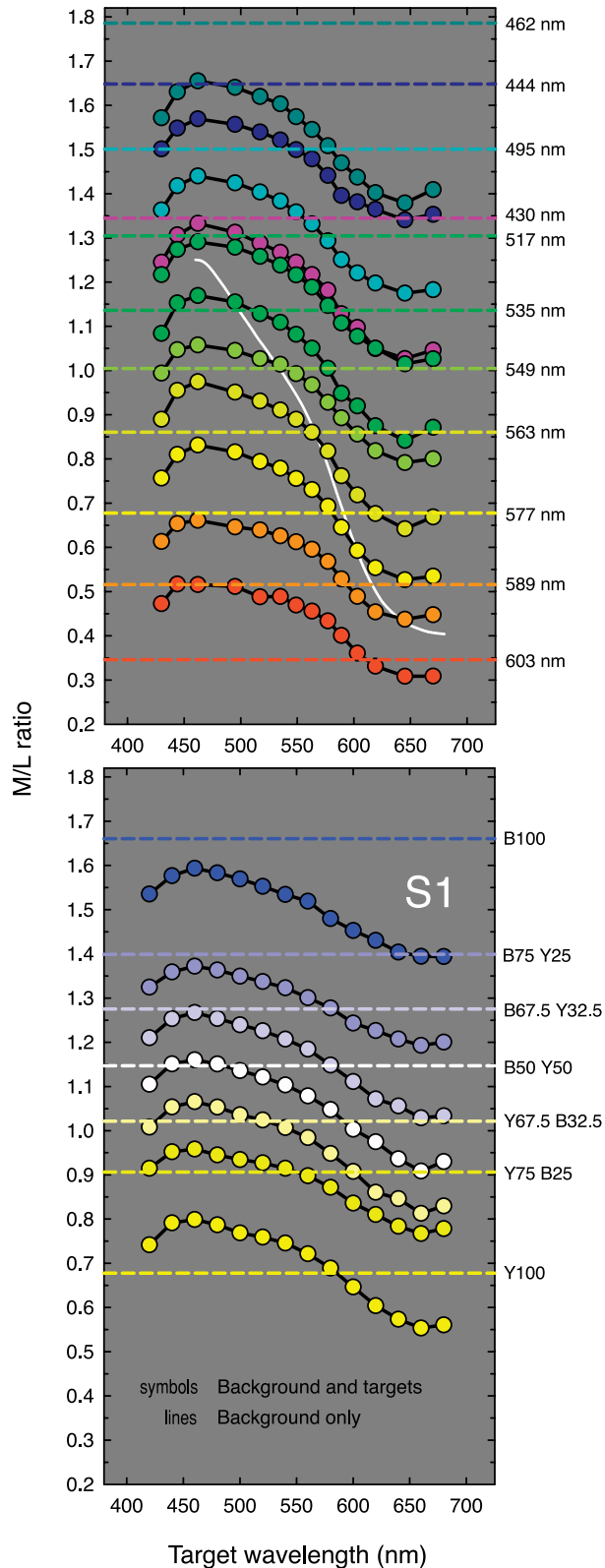
Because of these complexities, we have restricted our main analysis and model to data obtained on fields with wavelengths of 603 nm and shorter.

The flickering targets alter the mean adapting chromaticities

Even though the flickering 25-Hz targets and reference lights are each only about 0.2 log unit above threshold, they can significantly alter the mean adapting chromaticities. This influence is illustrated in Figure 3 for observer S1, who set the highest reference target threshold (for the other observers, the effects are smaller). The horizontal dashed lines in each panel show the ratios of M:L-cone excitations produced by the backgrounds or mixtures of backgrounds alone (M_{μ}/L_{μ}). Ideally, the mean chromaticity of the combined background, target, and reference lights at the HFP null ($M_{\mu,\lambda}/L_{\mu,\lambda}$) should deviate very little from the dashed lines. However, as the symbols show for subject S1, the mean chromaticity at each null (plotted as $M_{\mu,\lambda}/L_{\mu,\lambda}$) can diverge substantially from the chromaticity of the background alone. Overall, the target and reference lights shift the mean chromaticity of both short- and long-wavelength fields: $M_{\mu,\lambda}/L_{\mu,\lambda}$ is increased on short-wavelength fields and decreased on long-wavelength ones. Moreover, $M_{\mu,\lambda}/L_{\mu,\lambda}$ also changes with target wavelength (λ): $M_{\mu,\lambda}/L_{\mu,\lambda}$ is decreased by short-wavelength targets and increased by long-wavelength ones. This dependence of adapting field chromaticity on the test wavelength occurs on all backgrounds. Comparable effects can be seen for all six subjects in Figure 4, and Figures A1–A6 in Appendix A, in which the $M_{\mu,\lambda}/L_{\mu,\lambda}$ ratios produced by the background lights alone are shown by the vertical colored lines, and the combined values at each HFP null are shown by the symbols.

As discussed in detail in the next section, we account for the changes in background chromaticity by finding the

best-fitting linear combinations of the Stockman and Sharpe (2000) L- and M-cone fundamentals with respect to the relative M:L-cone excitation produced by the combined test, reference, and background lights ($M_{\mu,\lambda}/L_{\mu,\lambda}$ in Equations 2–5, below) calculated for each HFP setting.



Analysis of flicker photometric spectral sensitivity data

Mean HFP matches for six subjects

The mean 25-Hz HFP matches for subject S1 are shown in Figure 4 plotted as a function of the $M_{\mu,\lambda}/L_{\mu,\lambda}$ value for each HFP match. The matches for the other five subjects are shown in Figures A1–A6 in Appendix A. The matches were made in one run, except for observer S1, who made the bichromatic matches twice, and S2, who made the bichromatic and spectral matches twice, and observer A2, who made no bichromatic matches. The spectral matches and bichromatic mixture matches are shown in the upper and middle panels, respectively, in each figure, with the exception of those for observer S2, whose more extensive data span two figures: his first runs are shown in Appendix Figure A1, and his second in Appendix Figure A2.

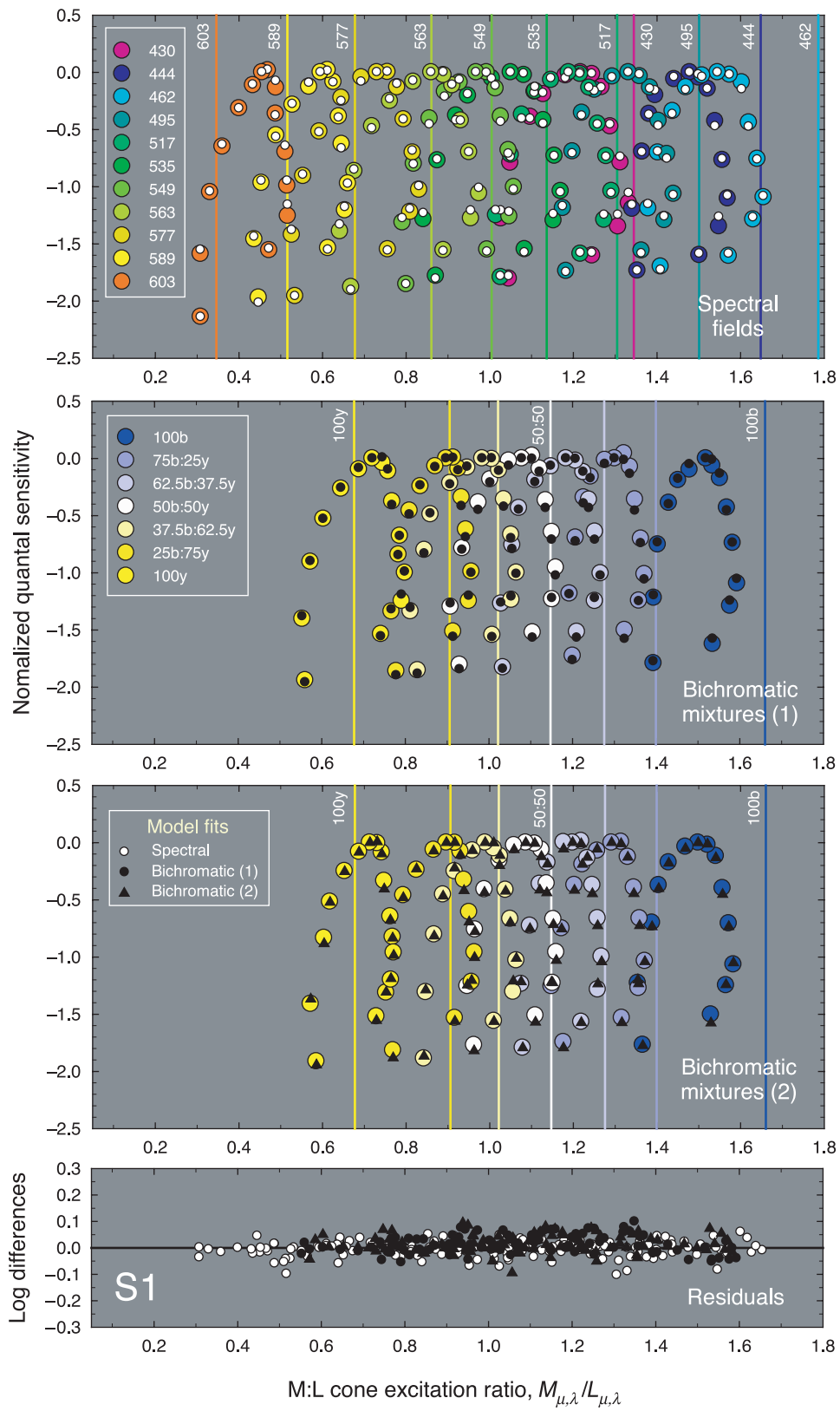
The spectral luminous efficiencies are plotted as a function of $M_{\mu,\lambda}/L_{\mu,\lambda}$ instead of as a conventional function of target wavelength, λ . This unusual scheme reveals the effects of the test and reference lights on the adapting chromaticity. Each spectral sensitivity curve, determined for the different spectral and bichromatic mixture fields, comprises the data for target wavelengths from 420 to 680 nm. Notice that the spectrum is effectively reversed in these plots. Long-wavelength backgrounds and targets produce lower $M_{\mu,\lambda}/L_{\mu,\lambda}$ values and therefore plot to the left, whereas shorter wavelength backgrounds and targets produce higher values and plot to the right. Consequently, the target wavelengths for each adapting condition plot from right to left.

The overall quality of the data is very good. The standard deviations within an observer are small and independent of test and field wavelength. Data are color-coded according to the approximate appearance of the adapting field. The small open (white dots) and closed (black dots) circles in the upper and middle panels are the model fits, which are described in the next section.

Model

In order to account for the changes in adapting chromaticity with μ and λ , we fit linear combinations of the Stockman and Sharpe (2000) L- and M-cone spectral

Figure 3. Mean M:L-cone excitation ratios elicited by the combined reference, target, and background lights ($M_{\mu,\lambda}/L_{\mu,\lambda}$) at each target wavelength for observer S1. The upper panel shows the ratios for the spectral backgrounds, and the lower panel shows those for the bichromatic mixtures. The dashed horizontal lines show the excitation ratios for the backgrounds alone (M_{μ}/L_{μ}). The backgrounds are identified by the labels to the right of each line, indicating either the adapting wavelength for the single fields or the proportion of Blue (B, 478 nm) to Yellow (Y, 577 nm) for the bichromatic fields. Symbols as Figures 1 and 2. The continuous white line in the upper panel shows the predicted ratios for a series of ERG 32.5-Hz flicker nulls (see Discussion section for details).



sensitivities for each adapting condition (μ) not just as a function of target wavelength (λ) but also as a function of the mean adapting chromaticity at each HFP null ($M_{\mu,\lambda}/L_{\mu,\lambda}$). We began with

$$\log_{10} V_{\mu} * (\lambda) = \log_{10}(a_{\mu} \bar{l}(\lambda) + \bar{m}(\lambda)), \quad (1)$$

where a_{μ} is the L-cone weight, $V_{\mu}^*(\lambda)$ is the predicted spectral sensitivity (luminous efficiency) function for an adapting field μ , $\bar{l}(\lambda)$ is either the L(ser¹⁸⁰) or the L(ala¹⁸⁰) variant of the Stockman and Sharpe (2000) L-cone fundamentals, and $\bar{m}(\lambda)$ is the Stockman and Sharpe (2000) M-cone spectral sensitivity. The spectral sensitivity functions, which in these formulae are quantum-based, are given in Appendix Table A1. We then set $a_{\mu} = \beta_{\mu} \times (M_{\mu,\lambda}/L_{\mu,\lambda})$, where β_{μ} is now the “L-cone bias,” and (to reiterate) $M_{\mu,\lambda}/L_{\mu,\lambda}$ is the relative M:L-cone excitation produced by the combined test, reference, and background lights at each HFP null. (We ignore the possibility that the M- and L-cone incremental test components might have a greater or lesser influence than expected, because of spatial opponency or spatial integration with respect to the surrounding background.) The excitation ratios were calculated from the radiometric calibrations and null settings using the Stockman & Sharpe cone fundamentals with unity quantal peaks. Next, the sensitivity for each μ , λ , and $M_{\mu,\lambda}/L_{\mu,\lambda}$ is normalized relative to the reference wavelength of 560 nm (recall that $M_{\mu,\lambda}/L_{\mu,\lambda}$ includes the effects of the fixed 560-nm reference), so that

$$\log_{10} V_{\mu} * (\lambda) = \log_{10} \left(\beta_{\mu} \frac{M_{\mu,\lambda}}{L_{\mu,\lambda}} \bar{l}(\lambda) + \bar{m}(\lambda) \right) - \log_{10} \left(\beta_{\mu} \frac{M_{\mu,\lambda}}{L_{\mu,\lambda}} \bar{l}(560) + \bar{m}(560) \right). \quad (2)$$

Figure 4. Luminous efficiencies (HFP matches), in decimal logarithm, versus M:L-cone excitation ratios elicited by the combined reference, test, and background lights ($M_{\mu,\lambda}/L_{\mu,\lambda}$) for observer S1. The upper panel shows the HFP sensitivities determined on the 11 spectral adapting fields. The second and third panels show two separate determinations of the HFP sensitivities on the 7 bichromatic, 478 nm (blue, b) + 577 nm (yellow, y) adapting fields. The small open circles (which appear as white dots), filled circles (which appear as black dots), and filled black triangles plotted, respectively, in the upper three panels are the best-fitting combinations of the Stockman and Sharpe (2000) M- and L-cone fundamentals determined from Equation 4. The corresponding residuals are plotted in the lowest panel. The M:L-cone excitation ratios produced by the labeled background adapting fields alone (M_{μ}/L_{μ}) are identified by the vertical colored lines in the upper three panels. Symbols as Figures 1–3 (see also key).

Equation 2 defines the sensitivity difference (or relative HFP match) between λ and 560 nm for each combination of background, test, and reference lights at an HFP null.

The reason we have added the complexity of setting $a_{\mu} = \beta_{\mu} \times (M_{\mu,\lambda}/L_{\mu,\lambda})$ is illustrated by rearranging (Equation 2) to yield

$$\log_{10} V_{\mu} * (\lambda) = \log_{10} \left(\beta_{\mu} \frac{\bar{l}(\lambda)}{L_{\mu,\lambda}} + \frac{\bar{m}(\lambda)}{M_{\mu,\lambda}} \right) - \log_{10} \left(\beta_{\mu} \frac{\bar{l}(560)}{L_{\mu,\lambda}} + \frac{\bar{m}(560)}{M_{\mu,\lambda}} \right). \quad (3)$$

In Equation 3, the L-cone fundamental is scaled by the L-cone excitation, and the M-cone fundamental is scaled by the M-cone excitation, which is equivalent to a reciprocal sensitivity adjustment of each cone signal in accordance with Weber’s Law. Consequently, if the L-cone bias, β_{μ} , is found to be constant over a range of $M_{\mu,\lambda}/L_{\mu,\lambda}$, it suggests that Weber’s Law holds over that range. An increase in β_{μ} implies a decrease of the M-cone contribution relative to the Weber’s Law prediction, whereas a decrease in β_{μ} implies a decrease of the L-cone contribution relative to the Weber’s Law prediction. Increases or decreases in β_{μ} can be potentially due to a variety of causes including relative chromatic suppression or facilitation, or shortfalls from Weber’s Law (see above).

We found the best-fitting values of β_{μ} for each spectral and bichromatic spectral sensitivity condition (μ) by simultaneously fitting all the data for each subject with

$$\log_{10} V_{\mu} * (\lambda) = \log_{10} \left(\beta_{\mu} \frac{M_{\mu,\lambda}}{L_{\mu,\lambda}} \bar{l}(\lambda) + \bar{m}(\lambda) \right) + k_{lens} d_{lens}(\lambda) + k_{mac} d_{mac}(\lambda) - \log_{10} \left(\beta_{\mu} \frac{M_{\mu,\lambda}}{L_{\mu,\lambda}} \bar{l}(560) + \bar{m}(560) \right) - k_{lens} d_{lens}(560) - k_{mac} d_{mac}(560). \quad (4)$$

Equation 4 is the same as Equation 2, except that the data for each subject undergo best-fitting adjustments for individual differences in prereceptoral lens and macular pigment filtering. The constants k_{lens} and k_{mac} are, respectively, best-fitting lens and macular pigment density multipliers that adjust each subject’s HFP curves to be consistent with the mean lens [$d_{lens}(\lambda)$] and macular [$d_{mac}(\lambda)$] pigment density spectra implied by the Stockman and Sharpe standard observer. The function $d_{lens}(\lambda)$ is the lens pigment density spectrum of Norren

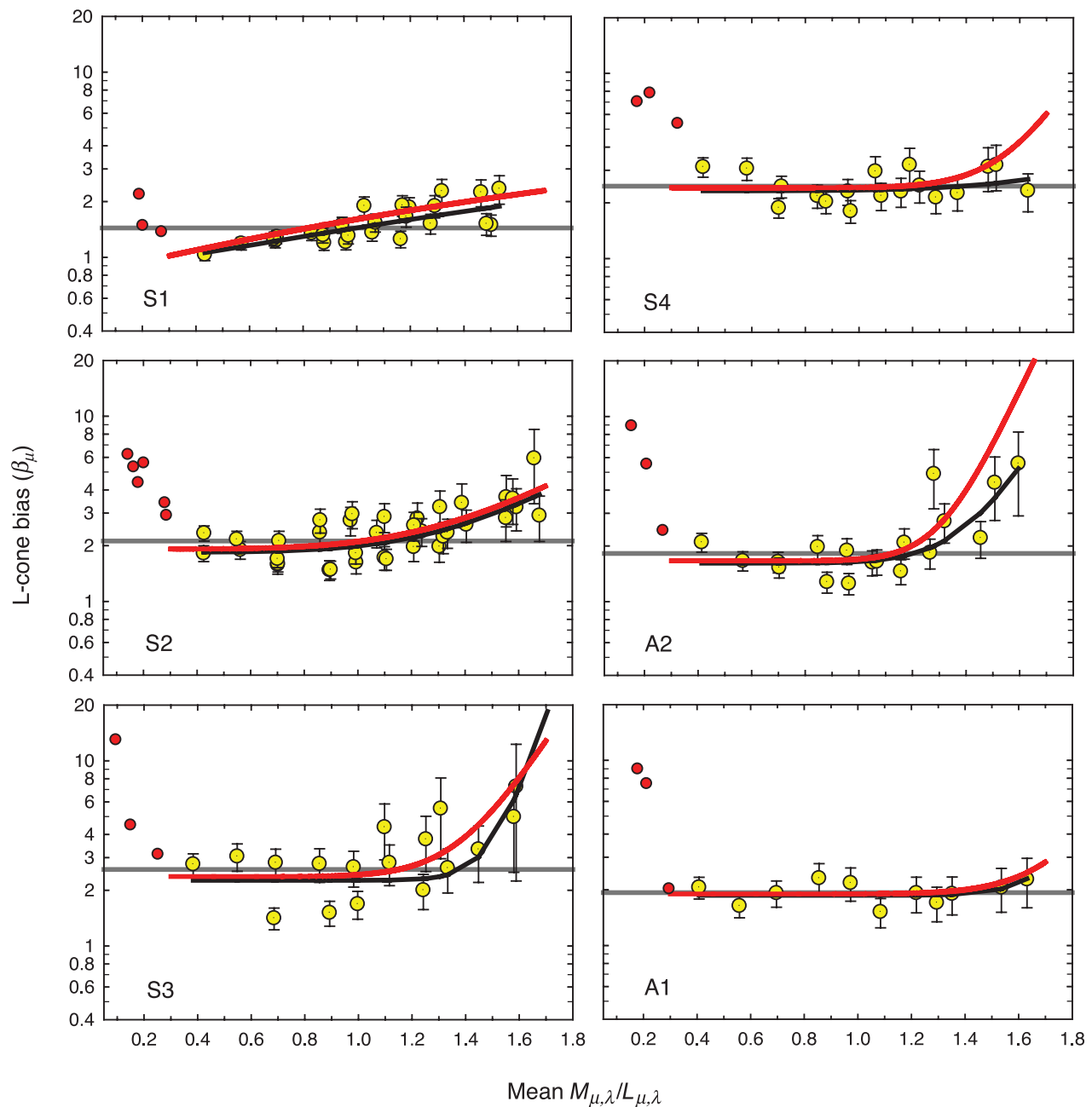


Figure 5. The best-fitting values of the L-cone bias, β_{μ} , for each of the six observers (Panels 1–6), plotted as a function of the mean $M_{\mu,\lambda}/L_{\mu,\lambda}$ cone excitations for each adapting and mixture field condition (dotted, yellow circles). The standard errors of the fits are indicated. The red circles in each panel show the partial results of a separate analysis that included the three longest wavelength backgrounds of 619, 645, and 670 nm, which were excluded from the main analysis. The continuous black lines indicate simple power functions (Equation 5) fitted to the dotted, yellow circles. The red continuous lines indicate best-fitting forms of the threshold power model (Equations 4 and 5) fitted simultaneously to each observer's HFP data for all background conditions. The horizontal gray lines indicate the best-fitting fixed L-cone bias (Weber's Law) again fitted simultaneously to each observer's HFP data for all background conditions.

and Vos (1974), slightly modified by Stockman, Sharpe, and Fach (1999) [$d_{lens}(400)$, for example, is 1.76], while the function $d_{mac}(\lambda)$ is the mean macular density spectrum based on measurements by Bone, Landrum, and Cairns (1992) proposed by Stockman et al. (1999) [$d_{mac}(460)$, for example, is 0.35]. For further details about the fitting

procedure, see our earlier papers (Sharpe et al., 2005; Stockman & Sharpe, 2000).

The appropriate L(ser^{180}) and L(ala^{180}) cone templates are based on the Stockman and Sharpe (2000) L-cone fundamental calculated back to an absorbance spectrum (see their Table 2, Column 9), and then shifted along a

logarithmic wavelength scale by -1.51 nm at λ_{\max} for L(ala¹⁸⁰) or by $+1.19$ nm for L(ser¹⁸⁰) in accordance with the 2.7-nm spectral shift between the L(ala¹⁸⁰) and L(ser¹⁸⁰) spectral sensitivities (Sharpe, Stockman, Jägle et al., 1998). Eisner and MacLeod (1981) also found a 2.7-nm shift between two groups of alleged L-cone isolates but of unknown genotype. The two respective shifted spectra were then corrected back to corneal spectral sensitivities to generate the corneal templates used in the fits. For further details, see Stockman and Sharpe (2000). These two templates, which have not been published before, are provided in 5-nm steps in Table A1 in Appendix A. The use of the appropriate version of the L-cone template is important for avoiding sizable errors that can arise in estimating the relative L-cone weights with the mean L-cone template (e.g., Bieber, Kraft, & Werner, 1998; Carroll, McMahon, Neitz, & Neitz, 2000; Sharpe et al., 2005). The functions in Equation 4 can be downloaded from the website: <http://www.cvrl.org>.

We used two approaches to fit Equation 4 simultaneously to all the data for each subject. First, we determined the optimal β_{μ} for each μ . Second, we assumed that β_{μ}

varied as some function of μ or was constant (Weber's Law) and determined the optimal fit for all μ .

Determination of β_{μ} for each μ

In these fits, the best-fitting values of β_{μ} were found for each adapting condition, μ , and the best-fitting values of k_{lens} and k_{mac} were found for each subject for all μ . The fits to the luminous efficiency data are shown in the upper and middle panels of Figure 4 and Appendix Figures A1–A6 as the small symbols in each panel, and the residuals are shown in the lower panels. Overall, the fits are good with R^2 values of better than 99% (see Table 1), but some systematic deviations are apparent. This suggests that the model of 25-Hz HFP-determined luminous efficiency embodied in Equation 4, which combines only L- and M-cone signals, is essentially correct.

Figure 5 shows the best-fitting values of the logarithm of the L-cone bias, β_{μ} , for each subject, plotted as a function of the mean $M_{\mu,\lambda}/L_{\mu,\lambda}$ for each condition (dotted, yellow circles). The best-fitting values, \pm their standard error, and the percentage coefficient of determination (R^2) are given in section (i) of Table 1.

	Serine 180				Alanine 180	
	S1	S2	S3	S4	A1	A2
(i) Separate determinations of β_{μ} for each μ						
k_{lens}	0.03 ± 0.01	-0.29 ± 0.02	0.07 ± 0.02	0.31 ± 0.02	0.22 ± 0.02	-0.06 ± 0.03
k_{mac}	-0.14 ± 0.02	-0.53 ± 0.02	-0.29 ± 0.03	-0.39 ± 0.02	-0.47 ± 0.02	-0.73 ± 0.04
rms error	0.034	0.038	0.049	0.041	0.043	0.049
R^2	99.70	99.66	99.31	99.50	99.50	99.14
(ii) β_{μ} constant (Weber's Law)						
β_{μ}	1.44 ± 0.06	2.12 ± 0.06	2.59 ± 0.16	2.46 ± 0.11	1.82 ± 0.08	1.93 ± 0.12
k_{lens}	0.03 ± 0.01	-0.29 ± 0.01	0.06 ± 0.02	0.31 ± 0.02	0.21 ± 0.02	-0.06 ± 0.03
k_{mac}	-0.13 ± 0.02	-0.54 ± 0.02	-0.30 ± 0.03	-0.39 ± 0.02	-0.48 ± 0.03	-0.73 ± 0.04
rms error	0.038	0.042	0.055	0.043	0.049	0.050
R^2	99.58	99.58	99.12	99.44	99.36	99.38
(iii) β_{μ} threshold power model						
n	0.84 ± 0.24	1.92 ± 0.08	2.37 ± 0.16	2.41 ± 0.12	1.67 ± 0.08	1.90 ± 0.13
b	1.21 ± 0.55	4.71 ± 1.44	9.90 ± 4.38	11.13 ± 7.88	1.24 ± 3.67	1.13 ± 25.90
c	1.08 ± 0.52	1.64 ± 0.09	1.46 ± 0.07	1.64 ± 0.11	1.36 ± 0.04	1.81 ± 0.56
k_{lens}	0.03 ± 0.01	-0.29 ± 0.01	0.06 ± 0.02	0.31 ± 0.02	0.21 ± 0.02	-0.06 ± 0.03
k_{mac}	-0.09 ± 0.02	-0.52 ± 0.02	-0.28 ± 0.03	-0.37 ± 0.02	-0.44 ± 0.02	-0.72 ± 0.04
rms error	0.035	0.041	0.053	0.043	0.045	0.050
R^2	99.66	99.61	99.20	99.46	99.46	99.39

Table 1. The best-fitting values \pm their standard errors, the rms error, and the percentage coefficient of determination (R^2) for each of the four L(ser¹⁸⁰)-cone, S1–S4, and two L(ala¹⁸⁰)-cone, A1 and A2, observers. The results of three fits are tabulated. For each fit, k_{lens} and k_{mac} are the best-fitting lens and macular adjustments as defined in Equation 4. These values correspond to the lens and macular pigment density differences between each observer and the standard observer represented by the Stockman and Sharpe (2000) M- and L-cone fundamentals. Fit (i): Separate determination of the L-cone bias β_{μ} for each adapting field μ and determination of k_{lens} and k_{mac} for all μ simultaneously. The best-fitting values of k_{lens} and k_{mac} are tabulated. Those of β_{μ} are not tabulated but are plotted in Figure 5 (yellow dotted circles). Fit (ii): A fixed value of β_{μ} was assumed for all μ (i.e., Weber's Law was assumed to hold). The best-fitting values of β_{μ} , k_{lens} , and k_{mac} are tabulated. Fit (iii): α_{μ} was assumed to grow as a function of $M_{\mu,\lambda}/L_{\mu,\lambda}$ raised to the power b , according to Equation 5. The best-fitting parameters of Equation 5, n , b and c , are tabulated, along with the simultaneously fitted values for k_{lens} and k_{mac} .

In general, β_μ is roughly constant at low $M_{\mu,\lambda}/L_{\mu,\lambda}$ (i.e., Weber's Law holds), but for four out of six subjects (S1, S2, S3, and A1) it increases at higher mean $M_{\mu,\lambda}/L_{\mu,\lambda}$ (i.e., the M-cone contribution falls below the Weber's Law prediction). The fall in the M-cone contribution on shorter wavelength fields (lower mean $M_{\mu,\lambda}/L_{\mu,\lambda}$) is expected from previous work (e.g., Eisner & MacLeod, 1981). Note that although the L-cone bias, β_μ , is constant at low $M_{\mu,\lambda}/L_{\mu,\lambda}$, the weight, a_μ , decreases as $M_{\mu,\lambda}/L_{\mu,\lambda}$ decreases. In general, on shorter wavelength fields (i.e., higher values of $M_{\mu,\lambda}/L_{\mu,\lambda}$), a_μ increases so that the spectral luminous efficiency becomes more L-cone-like, whereas on longer wavelength fields (i.e., lower values of $M_{\mu,\lambda}/L_{\mu,\lambda}$), it decreases so that the efficiency becomes more M-cone-like (compare the red and black continuous lines in Figure 6, below).

Notice that as β_μ increases, so too does the standard error of its fit. This is a general property of these fits that arises because as β_μ gets larger, its effect on spectral sensitivity gets smaller (for further discussion, see Sharpe et al., 2005). Thus, apparently large discrepancies between large values of β_μ , such as that between the two β_μ values for the repeated 462-nm adapting field measurements for S2 (i.e., the two rightmost yellow circles in the middle left panel of Figure 5), correspond to only relatively small differences in the underlying spectral luminous efficiency functions.

The mean values of k_{lens} were 0.03, -0.29 , 0.07, 0.31, 0.22, and -0.05 for subjects S1–S4, A1, and A2, respectively, and the mean values of k_{mac} were -0.14 , -0.53 , -0.29 , -0.39 , -0.47 , and -0.73 , respectively. These values correspond to the factor by which the pigment density spectrum template in question must be adjusted to bring each subject's luminous efficiency data into best agreement with the linear combination of $\bar{l}(\lambda)$ and $\bar{m}(\lambda)$. Note that a negative value means that a particular subject has a higher pigment density than the Stockman and Sharpe (2000) mean observer, and a positive value, a lower pigment density. Thus, our observers have on average 0.05 times less lens density as the Stockman and Sharpe (2000) mean observer (so that their mean density at 400 nm is 1.67 compared with 1.76) and, on average, 0.43 times more macular density (so that their mean peak density is 0.50 compared with 0.35). Our observers, therefore, are more heavily macular pigmented, on average, than the Stockman and Sharpe (2000) mean observer, but their density values all lie within the normal range. We are confident that these densities are not overinflated by the fitting procedure. The macular pigment density of three of the six subjects has been estimated before. Two of them (S2 and A2) participated in a study (Sharpe, Stockman, Knau, & Jägle, 1998) in which the actual macular density spectra were determined. S2 was found to have a peak density of 0.50 (compared with 0.54 here) and A2 was found to have a peak density of approximately 0.60 (compared with 0.61 here). S1 has carried out more limited determinations but is known to be typical in having a peak density of ca. 0.35 (compared with 0.40 here).

The red circles in each panel of Figure 5 show the partial results of a separate analysis that included the three longest wavelength backgrounds of 619, 645, and 670 nm, which were excluded from the main analysis. As the field wavelength lengthens, β_μ becomes increasingly large, suggesting the contribution of the M-cones falls below the Weber's Law predictions. However, this is one of the complexities discussed in The effects of background luminance section; the lowered M-cone contribution occurs probably because the M-cones are relatively unadapted.

Determination of β_μ as a function of μ

By using Equation 4 and separately determining β_μ for each μ , we have effectively assumed that local variations of $M_{\mu,\lambda}/L_{\mu,\lambda}$ around the mean for each adapting condition induce changes in the L-cone weight that are consistent with Weber's Law (i.e., we assume that, locally, β_μ is constant). The goodness of the fits shown in Figure 4 and Appendix Figures A1–A6 suggests that this is a reasonable approximation. However, for the majority of subjects the β_μ values, as shown in Figure 5, increase as $M_{\mu,\lambda}/L_{\mu,\lambda}$ increases. In this section, we try to capture this increase by assuming that β_μ increases as some function of $M_{\mu,\lambda}/L_{\mu,\lambda}$. In principle, this should yield a better local fit in those regions in which $M_{\mu,\lambda}/L_{\mu,\lambda}$ increases.

Initially, however, we made the much simpler assumption that Weber's Law holds across all conditions, and that β_μ is therefore fixed across all $M_{\mu,\lambda}/L_{\mu,\lambda}$. Equation 4 was fitted simultaneously to all the data for each subject to find the best-fitting values of β_μ , k_{lens} , and k_{mac} for all μ . This reduced the number of fitted parameters from 20 (or more for S1 and S2, less for A1) to just 3. Figure 5 shows the best-fitting values of the fixed L-cone bias, β_μ , for each subject, plotted as a horizontal gray line. The best-fitting values, \pm their standard error, and the percentage coefficient of determination (R^2) are given in section (ii) of Table 1. Despite the large reduction in the number of parameters, the fits are only slightly worse than the individual fits. However, the fixed value clearly underestimates β_μ at low $M_{\mu,\lambda}/L_{\mu,\lambda}$ values and overestimates it at high values, which is undesirable in any predictive model. To overcome this problem, we sought a simple continuous function that could be used to describe the change in β_μ for all 6 subjects just by changing its parameters. We finally settled on the following version of a power function:

$$\beta_\mu = n \left(1 + \left[\frac{M_{\mu,\lambda}/L_{\mu,\lambda}}{c} \right]^b \right), \quad (5)$$

in which b is the power to which $M_{\mu,\lambda}/L_{\mu,\lambda}$ is raised, c determines the "threshold" level of $M_{\mu,\lambda}/L_{\mu,\lambda}$ after which the power term becomes important, and n is a multiplier that scales the whole function.

Equation 5 is shown as the continuous black lines in Figure 5 fitted to the individual β_μ estimates for each

subject (dotted yellow circles). This fit was weighted according to the reciprocal of the standard errors of β_μ . Weighting the fits in this way is important because, as β_μ (or a_μ) increases, so too does its standard error (see Figure 7 of Sharpe et al., 2005). As can be seen, the same function does a reasonable job of characterizing the change in β_μ with $M_{\mu,\lambda}/L_{\mu,\lambda}$ for all six subjects.

Rather than finding the best-fitting parameters of Equation 5 by fitting it to estimates of β_μ shown in Figure 5, we next determined the best-fitting parameters *directly* from the HFP data. To achieve this, we inserted Equation 5 into Equation 4, and found for each subject the best-fitting values of n , c , b , k_{lens} and k_{mac} for all μ . The best-fitting values, \pm their standard error, and the percentage coefficient of determination (R^2) are given in section (iii) of Table 1. Figure 5 shows the best-fitting form of Equation 5 as the red continuous lines. The goodness of this fit is intermediate between the fixed β_μ fits and the fits in which β_μ values were determined for each μ . Indeed, the combination of Equations 4 and 5 provides a reasonably simple description of the 25 HFP data for each subject using just five parameters.

Discussion

We have been able to model the luminous efficiency data for each subject successfully either by individually determining L-cone bias factor β_μ for each effective background wavelength μ , or by assuming that β_μ varies as some simple function of $M_{\mu,\lambda}/L_{\mu,\lambda}$. We can extend this model to predict luminous efficiency of a “typical” observer, by linking it to the mean luminous efficiency data of Sharpe et al. (2005).

$V_\mu^*(\lambda)$ for a “typical” observer

We define $V_\mu^*(\lambda)$ for a typical observer according to

$$\log_{10} V_\mu^*(\lambda) = \log_{10} \left(\beta_\mu \frac{M_\mu}{L_\mu} \bar{l}(\lambda) + \bar{m}(\lambda) \right) - c_\mu, \quad (6)$$

in which c_μ is simply a unity normalizing constant that varies with μ and can be calculated once the other parameters are known (it is, in fact, the value of the first part of the equation when λ equals λ_{max} , the wavelength of peak efficiency). Note that in defining these formulae, the luminous efficiency and the state of adaptation are assumed to be *independent* of λ . As for our six individual observers, we use Equation 5 to define how β_μ in Equation 6 changes with M_μ/L_μ . But, which values of n , c , and b are appropriate for the typical observer represented by the $V^*(\lambda)$ function (Sharpe et al., 2005)? Note that an L-cone

weight (a_μ) of 1.55 was initially determined for the $V^*(\lambda)$ function. However, the analyses carried out for this paper made clear that the mean adapting chromaticity had also varied as a function of target wavelength in the earlier $V^*(\lambda)$ measurements. Accordingly, we have reanalyzed the original $V^*(\lambda)$ data making appropriate corrections. In relative quantal units, with $\bar{l}(\lambda)$ and $\bar{m}(\lambda)$ both normalized to unity quantal peak, $a = 1.89$, while in relative energy terms, with $\bar{l}(\lambda)$ and $\bar{m}(\lambda)$ normalized to unity energy peak, $a = 1.98$. These values supersede the values of 1.55 and 1.62 for quantal and energy units, respectively, given in the original paper (Sharpe et al., 2005). Given this reassessment, the luminous efficiency measurements obtained in 40 observers on a daylight D₆₅ field (Sharpe et al., 2005) suggest that $\beta_\mu \times M_\mu/L_\mu$ (or a_μ) should equal 1.89, and thus β_μ should equal 2.29, for the standard observer.

The value of β_μ of 2.29 ties Equation 5 at one value of M_μ/L_μ , but what about the other parameter values? Our solution is to take advantage of the common feature of the individual β_μ versus $M_{\mu,\lambda}/L_{\mu,\lambda}$ functions across subjects (see Figure 6); namely, that the functions are roughly constant at low $M_{\mu,\lambda}/L_{\mu,\lambda}$ (i.e., they follow Weber’s Law). Figure 6 shows these individual functions unaligned in the upper panel and vertically aligned at $M_{\mu,\lambda}/L_{\mu,\lambda} < 1$ in the lower panel. The alignment was achieved by scaling the functions and minimizing the squared differences between them and the mean. The fit of Equation 5 to the aligned data was weighted by the reciprocal of the standard errors shown in the figure. The best-fitting version of Equation 5 to account for the aligned data was then found. It is shown by the red line in Figure 6 and is given by

$$\beta_\mu = n \left(1 + \left[\frac{M_\mu/L_\mu}{1.7964} \right]^{3.6748} \right) \quad (7)$$

with $n = 2.1699$ (n is left undefined in the equation, because it can be allowed to vary for individual subjects). The vertical position of the aligned functions in the lower panel of Figure 6 was chosen so that Equation 7 with $n = 2.1699$ is equal to 2.29 for a D₆₅ background (as indicated by the vertical and upper dashed horizontal lines in Figure 6). The L-cone weights, a_μ , corresponding to Equation 7 with $n = 2.1699$ are shown by the continuous black line. As required by $V_{D65}^*(\lambda)$, a_{D65} is equal to 1.89 (as indicated by the vertical and lower dashed horizontal lines).

We propose Equations 6 and 7 as the definition of $V_\mu^*(\lambda)$ for a typical observer. As in Equation 6, M_μ/L_μ in Equation 7 is assumed for the general formulae to be independent of λ . To implement this combined equation, M_μ/L_μ , the ratio of the M:L-cone excitations, must be computed for each adapting condition. For monochromatic or nearly monochromatic lights, this value can simply be read off Table A1 for the L(mean)-cone template or for the appropriate L(ser¹⁸⁰)- or L(ala¹⁸⁰)-cone template when the relevant polymorphic variant is known. For spectrally complex lights, the ratio must be

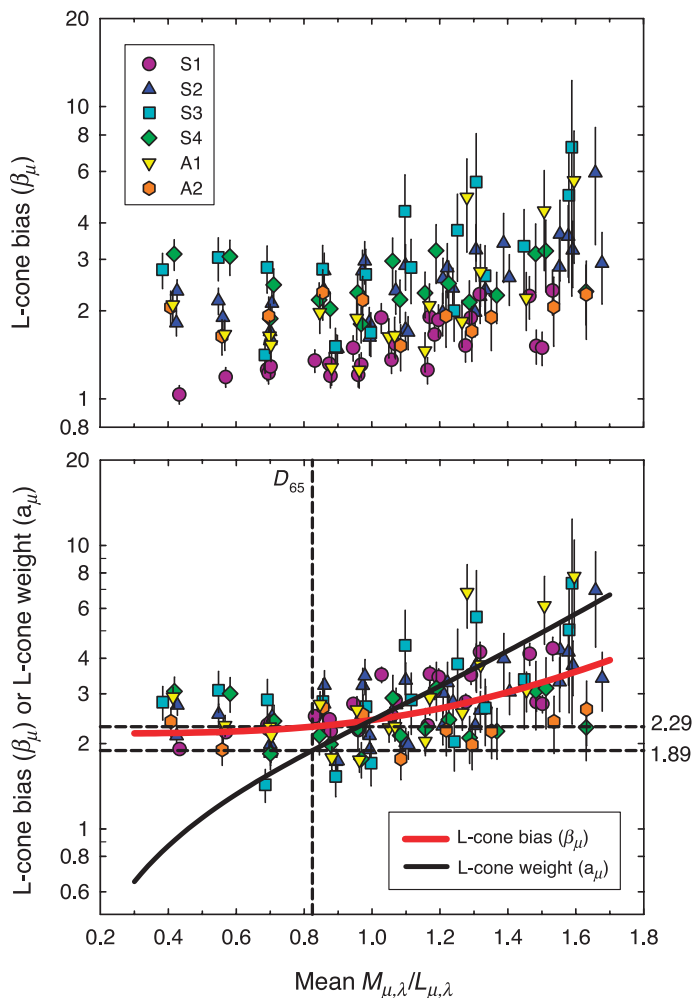


Figure 6. The L-cone bias (β_{μ}) as a function of mean M_{μ}/L_{μ} cone excitation for each of the six observers (different colored symbols) unaligned (top panel) and vertically aligned at $M_{\mu}/L_{\mu} < 1$ (bottom panel). The red line denotes the $V_{\mu}^*(\lambda)$ L-cone bias “template” function (see description of Equation 7 in the text for details), and the black line the corresponding L-cone weights. The dashed lines indicate the L-cone bias and L-cone weight template values corresponding to the $M_{\mu,\lambda}/L_{\mu,\lambda}$ cone excitation ratio for a D_{65} white field.

calculated by cross-multiplying the spectral power distribution of the field in question with the Stockman and Sharpe (2000) L- and M-cone spectral sensitivities (after choosing the appropriate L-cone polymorphic variant), separately summing the L- and M-cone cross-multiplications and obtaining the ratio between them. For the estimate of $V_{\mu}^*(\lambda)$ to be more accurate for individual observers, n in Equation 7 can be individually determined.

Chromatic suppression of the cone inputs to luminance

Evidence that the luminance contribution of the L- or M-cone type more sensitive to a given chromatic

field is suppressed in excess of Weber’s Law has been presented before (Eisner & MacLeod, 1981; Stockman et al., 1993), although in one study the L-cone suppression on long-wavelength fields was found to be more pronounced than M-cone suppression on short-wavelength ones (Stromeyer et al., 1987). Such suppression causes luminous efficiency functions to become more M-cone-like than expected on long-wavelength adapting fields and more L-cone-like than expected on short-wavelength fields.

Our results are consistent with a relative M-cone suppression in excess of Weber’s Law on short-wavelength fields but with there being no comparable L-cone suppression on long-wavelength fields. The apparent lack of L-cone suppression (red circles, Figure 5) may simply reflect the low levels of M-cone adaptation on 3 log troland long-wavelength fields (see, e.g., De Vries, 1948b; Eisner & MacLeod, 1981; Stiles, 1978; Stockman et al., 1993; Stockman, Montag, & Plummer, 2006; Stromeyer et al., 1987).

It is important to note that obedience to the Weber’s Law prediction does not necessarily imply an absence of chromatic suppression. For example, on longer wavelength fields, such as 603 nm, Weber’s Law for M-cone flicker detection in normal trichromats may reflect a less-than-Weber adjustment of 25-Hz gain at the cone level, with a later, cone-opponent suppression of the M-cone signal. The expected relative suppression on long-wavelength fields is, however, of the L-cones (Eisner & MacLeod, 1981).

Another complication is that the L- and M-cone suppressions, particularly on long-wavelength fields, may be due in part to constructive and destructive interference between the fast and slow M- and L-cone signals (Stockman, Montag et al., 2006; Stockman & Plummer, 2005a, 2005b; Stockman et al., 2005). These interference effects are most prominent near 15 Hz. Consequently, the use of 25-Hz flicker would have reduced any effects of interference.

Luminous efficiency and relative L- and M-cone numerosity

Luminous efficiency functions have been used by several groups as a way of estimating the relative number of L- and M-cones in the retinal area within which it is measured (e.g., Adam, 1969; Crone, 1959; De Vries, 1946, 1948a; Dobkins, Thiele, & Albright, 2000; Gunther & Dobkins, 2002; Kremers, Scholl, Knau, Berendschot, & Sharpe, 2000; Lutze, Cox, Smith, & Pokorny, 1990; Rushton & Baker, 1964; Smith & Pokorny, 1975; Vimal, Pokorny, Smith, & Shevell, 1989; Vos & Walraven, 1971). The assumption underlying such estimates is that the L-cone weight $a_{\mu}(\beta_{\mu} \times M_{\mu,\lambda}/L_{\mu,\lambda})$, in our model) directly reflects the relative numbers of the

L- and M-cones contributing to luminous efficiency. This assumption is, however, highly questionable, because the outputs of each cone type are modified not only by receptor adaptation, but also, as our results suggest on short-wavelength fields that show M-cone suppression, by postreceptor adaptation before the signals are combined. Indeed, the strong dependence of a_μ on chromatic adaptation begs the question of which condition of chromatic adaptation should be considered truly “neutral”—in the sense of not altering the relative contributions of the M- and L-cones to luminous efficiency away from those due to relative numerosity. One way of potentially simplifying the problem is, as we have done, to consider the effects of selective proportional chromatic adaptation separately from other factors by considering the L-cone weight a_μ as $\beta_\mu \times M_{\mu,\lambda}/L_{\mu,\lambda}$, where β_μ is the L-cone bias. Indeed, it is tempting to conclude that the roughly constant value of β_μ found for low $M_{\mu,\lambda}/L_{\mu,\lambda}$ (where Weber’s Law approximately holds) actually reflects relative L- and M-cone numerosity.

However, even at low $M_{\mu,\lambda}/L_{\mu,\lambda}$, β_μ is still likely to be influenced by factors other than numerosity, such as neural weighting differences. In principle, β_μ could have little or nothing to do with relative L- and M-cone numbers but instead reflect the relative L- and M-cone contrast gains. This view is doubtful, however, given that L:M-cone ratio estimates derived from luminous efficiency functions correlate with estimates derived in the same subjects using other methods (e.g., Albrecht, Jägle, Hood, & Sharpe, 2002; Brainard et al., 2000; Kremers et al., 2000; Lutze et al., 1990; Rushton & Baker, 1964; Sharpe, de Luca, Hansen, Jägle, & Gegenfurtner, 2006; Vimal et al., 1989; Wesner, Pokorny, Shevell, & Smith, 1991). Nevertheless, any claims that luminous efficiency can be used to derive cone numerosity directly should be treated with extreme caution. Other workers have pointed out the problems of linking luminous efficiency with cone numerosity (e.g., Chaparro, Stromeyer, Kronauer, & Eskew, 1994; Eskew, McLellan, & Giulianini, 1999).

Backgrounds and HFP

The use of steady backgrounds mitigates against the changes in chromaticity caused by the 25-Hz reference and target lights. Had we not used backgrounds, the chromaticity changes would have been much larger. The problems caused by not using backgrounds for high-frequency HFP are nicely illustrated by the large body of ERG work carried out using 32.5-Hz flicker (e.g., Brainard et al., 2000; Carroll et al., 2000; Carroll, Neitz, & Neitz, 2002; Hofer, Carroll, Neitz, Neitz, &

Williams, 2005; Jacobs, Neitz, & Krogh, 1996). In these measurements, only two flickering fields of 59 deg in diameter were used: a flickering white (2850 K) reference field of 2.37 log trolands that was superimposed on a flickering variable-wavelength target, the radiance of which was adjusted to elicit a null in the ERG at 32.5 Hz. The white field, which was produced in Maxwellian-view by a tungsten halide lamp, had a color temperature close to Illuminant A. From the information provided, we can only roughly estimate the effects of this light on the M- and L-cones. However, a comparable spectrally calibrated white field (close to Illuminant A) of 2.37 log trolands in our system produced M:L-cone excitations equivalent to a monochromatic light of 578 nm and 8.35 log quanta·s⁻¹·deg⁻². Given this assumption, we can use the $V_\mu^*(\lambda)$ function to estimate the ERG flicker matches and then calculate from those matches the changes in adapting chromaticity with target wavelength. The estimated chromaticities for the ERG measurements are shown as the continuous white line in the upper panel of Figure 3. As can be seen, the changes in adapting chromaticity are substantial—much larger than the changes found when a background is used. Over the typical range of their ERG measurements (460 to 680 nm), the M/L cone excitation ratio changes from 1.25 (equivalent to a background of about 520 nm) to 0.40 (equivalent to a background of about 600 nm). These considerable changes in adapting chromaticity with target wavelength will distort the ERG spectral sensitivities (see Figure 2, above, for the expected changes between comparable spectral fields). The 32.5-Hz ERG measurements, therefore, are unlikely to reflect accurately relative L- and M-cone numerosity, as the authors claim. Although the curves may still be describable as a linear combination of the M- and L-cone spectral sensitivities (as we also found in a preliminary analysis of the HFP data shown here), the weights will be systematically offset from values that would be obtained if there had been no change in chromatic adaptation with target wavelength. Errors of this type are expected from the work of De Vries (1948b), who showed HFP additivity failures for combined test and reference targets that exceeded 1.7 log trolands.

As we noted above, any luminous efficiency function strictly applies only to the conditions of chromatic adaptation under which it was measured. In addition, the function will also depend on other aspects of the measurement: for example, the stimulus size, the stimulus intensity, the retinal location probed, the flicker frequency, the measurement task, and so on. These dependencies mean that any generalization of luminous efficiency will inevitably be an approximation. Indeed, if the measure of luminance is in any way critical, it should be determined anew for the particular conditions of interest.

Appendix A: Online appendix

L- and M-cone spectral sensitivities

nm	log M	log Lmean	M/Lmean	log L(<i>ser</i> ¹⁸⁰)	M/L(<i>ser</i> ¹⁸⁰)	log L(<i>ala</i> ¹⁸⁰)	M/L(<i>ala</i> ¹⁸⁰)
390	-3.2908	-3.2186	0.8470	-3.2459	0.9018	-3.2024	0.8159
395	-2.8809	-2.8202	0.8696	-2.8197	0.8686	-2.8119	0.8531
400	-2.5120	-2.4660	0.8994	-2.4737	0.9155	-2.4738	0.9158
405	-2.2013	-2.1688	0.9279	-2.1722	0.9352	-2.1746	0.9403
410	-1.9346	-1.9178	0.9622	-1.9245	0.9771	-1.9270	0.9828
415	-1.7218	-1.7371	1.0358	-1.7353	1.0316	-1.7368	1.0351
420	-1.5535	-1.6029	1.1206	-1.5999	1.1129	-1.5995	1.1119
425	-1.4235	-1.5136	1.2305	-1.5149	1.2342	-1.5120	1.2262
430	-1.3033	-1.4290	1.3357	-1.4345	1.3527	-1.4288	1.3350
435	-1.1900	-1.3513	1.4499	-1.3637	1.4921	-1.3548	1.4617
440	-1.0980	-1.2842	1.5355	-1.2938	1.5698	-1.2815	1.5259
445	-1.0342	-1.2414	1.6113	-1.2500	1.6436	-1.2343	1.5852
450	-0.9794	-1.2010	1.6659	-1.2085	1.6946	-1.1895	1.6222
455	-0.9319	-1.1606	1.6931	-1.1683	1.7234	-1.1463	1.6385
460	-0.8632	-1.0974	1.7144	-1.1113	1.7702	-1.0868	1.6734
465	-0.7734	-1.0062	1.7093	-1.0260	1.7889	-0.9996	1.6835
470	-0.6928	-0.9200	1.6873	-0.9395	1.7647	-0.9118	1.6557
475	-0.6301	-0.8475	1.6498	-0.8597	1.6968	-0.8313	1.5895
480	-0.5747	-0.7803	1.6052	-0.7913	1.6464	-0.7628	1.5421
485	-0.5235	-0.7166	1.5602	-0.7289	1.6050	-0.7010	1.5051
490	-0.4738	-0.6535	1.5125	-0.6626	1.5446	-0.6358	1.4520
495	-0.4078	-0.5730	1.4628	-0.5874	1.5120	-0.5620	1.4262
500	-0.3337	-0.4837	1.4126	-0.4980	1.4597	-0.4744	1.3825
505	-0.2569	-0.3929	1.3677	-0.4068	1.4122	-0.3852	1.3436
510	-0.1843	-0.3061	1.3238	-0.3191	1.3640	-0.2995	1.3039
515	-0.1209	-0.2279	1.2791	-0.2401	1.3157	-0.2226	1.2638
520	-0.0699	-0.1633	1.2397	-0.1789	1.2851	-0.1635	1.2403
525	-0.0389	-0.1178	1.1991	-0.1310	1.2363	-0.1176	1.1987
530	-0.0191	-0.0830	1.1586	-0.0914	1.1811	-0.0799	1.1501
535	-0.0081	-0.0571	1.1197	-0.0638	1.1369	-0.0540	1.1116
540	-0.0004	-0.0330	1.0779	-0.0421	1.1007	-0.0340	1.0803
545	-0.0036	-0.0187	1.0353	-0.0254	1.0516	-0.0189	1.0359
550	-0.0163	-0.0128	0.9918	-0.0131	0.9925	-0.0082	0.9813
555	-0.0295	-0.0050	0.9452	-0.0054	0.9460	-0.0021	0.9387
560	-0.0514	-0.0019	0.8923	-0.0017	0.8919	0.0000	0.8884
565	-0.0769	-0.0001	0.8379	0.0000	0.8377	0.0000	0.8377
570	-0.1115	-0.0015	0.7763	-0.0014	0.7761	-0.0033	0.7795
575	-0.1562	-0.0086	0.7119	-0.0062	0.7079	-0.0101	0.7143
580	-0.2143	-0.0225	0.6430	-0.0146	0.6315	-0.0209	0.6406
585	-0.2753	-0.0325	0.5718	-0.0282	0.5662	-0.0370	0.5778
590	-0.3443	-0.0491	0.5067	-0.0462	0.5034	-0.0579	0.5171
595	-0.4264	-0.0727	0.4429	-0.0693	0.4395	-0.0843	0.4549
600	-0.5198	-0.1026	0.3826	-0.1000	0.3803	-0.1186	0.3970
605	-0.6247	-0.1380	0.3261	-0.1357	0.3243	-0.1583	0.3416
610	-0.7390	-0.1823	0.2776	-0.1790	0.2755	-0.2060	0.2931

Table A1. The L(*ser*¹⁸⁰)- and L(*ala*¹⁸⁰)-cone templates based on the Stockman and Sharpe (2000) cone sensitivity measurements, which are tabulated here for the first time, as well as the L(mean)- and M-cone templates (from Stockman & Sharpe, 2000). Also tabulated are the M:L cone sensitivity ratios as a function of wavelength for the L(mean)-, L(*ser*¹⁸⁰)-, and L(*ala*¹⁸⁰)-cone template variants. Please note that all sensitivities are in quantal units.

nm	log M	log Lmean	M/Lmean	log L(ser ¹⁸⁰)	M/L(ser ¹⁸⁰)	log L(ala ¹⁸⁰)	M/L(ala ¹⁸⁰)
615	-0.8610	-0.2346	0.2364	-0.2295	0.2336	-0.2611	0.2512
620	-0.9915	-0.2943	0.2008	-0.2885	0.1982	-0.3252	0.2156
625	-1.1294	-0.3603	0.1702	-0.3555	0.1683	-0.3975	0.1854
630	-1.2721	-0.4421	0.1479	-0.4296	0.1437	-0.4771	0.1603
635	-1.4205	-0.5327	0.1295	-0.5121	0.1235	-0.5652	0.1395
640	-1.5748	-0.6273	0.1128	-0.6031	0.1067	-0.6618	0.1222
645	-1.7370	-0.7262	0.0976	-0.7046	0.0928	-0.7690	0.1076
650	-1.8900	-0.8407	0.0893	-0.8143	0.0840	-0.8844	0.0987
655	-2.0523	-0.9658	0.0819	-0.9311	0.0756	-1.0066	0.0900
660	-2.2220	-1.0966	0.0749	-1.0566	0.0683	-1.1375	0.0823
665	-2.3923	-1.2327	0.0692	-1.1904	0.0628	-1.2764	0.0766
670	-2.5559	-1.3739	0.0658	-1.3311	0.0596	-1.4219	0.0734
675	-2.7194	-1.5208	0.0633	-1.4779	0.0573	-1.5731	0.0714
680	-2.8843	-1.6736	0.0616	-1.6303	0.0557	-1.7294	0.0700
685	-3.0519	-1.8328	0.0604	-1.7874	0.0544	-1.8900	0.0689
690	-3.2234	-1.9992	0.0597	-1.9484	0.0531	-2.0539	0.0677
695	-3.3874	-2.1596	0.0592	-2.1124	0.0531	-2.2201	0.0680
700	-3.5484	-2.3200	0.0591	-2.2783	0.0537	-2.3876	0.0691
705	-3.7103	-2.4819	0.0591	-2.4452	0.0543	-2.5552	0.0700
710	-3.8757	-2.6490	0.0593	-2.6118	0.0545	-2.7217	0.0702
715	-4.0389	-2.8165	0.0599	-2.7769	0.0547	-2.8859	0.0703
720	-4.1981	-2.9801	0.0605	-2.9394	0.0551	-3.0466	0.0705
725	-4.3559	-3.1432	0.0613	-3.0979	0.0552	-3.2025	0.0702
730	-4.5101	-3.3032	0.0621	-3.2514	0.0551	-3.3525	0.0696
D ₆₅ *			0.8170		0.8200		0.8280
A*			0.6590		0.6560		0.6750

Table A1. (continued)

HFP matches

Mean 25-Hz HFP matches for subjects S2–S4, A1, and A2 plotted as a function of the $M_{\mu,\lambda}/L_{\mu,\lambda}$ value for each HFP match. **Figures A1** and **A2** show the repeated matches for subject S2, who made the bichromatic and

spectral matches twice. **Figures A3–A6** show the matches for S3, S4, A1, and A2, respectively. The spectral matches and bichromatic mixture matches are shown in the upper and middle panels, respectively, in each figure, with the exception of the figure for A2, who made no bichromatic matches. Data for S1 are shown in **Figure 4** in the main text.

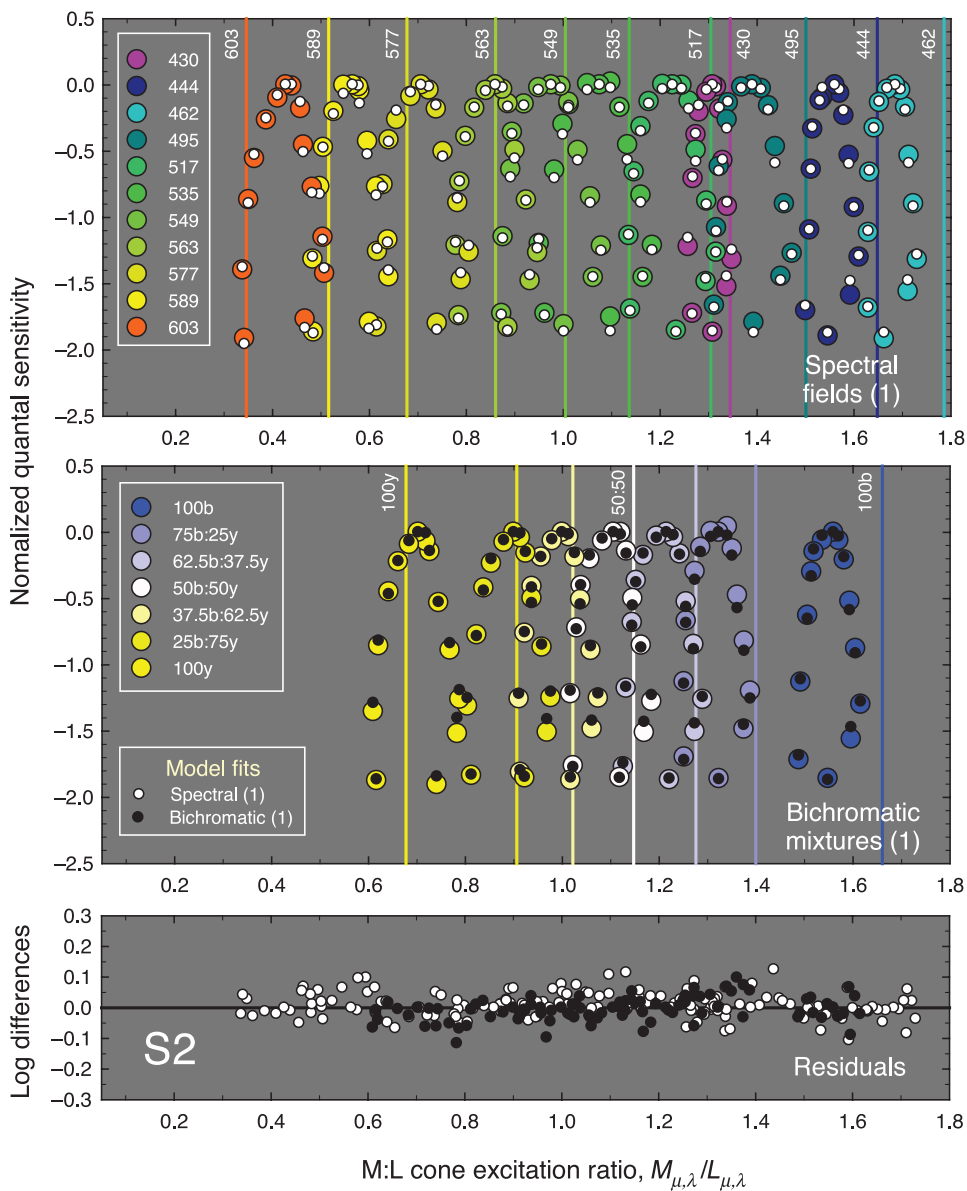


Figure A1. Luminous efficiencies (HFP matches) versus M:L-cone excitation ratios elicited by the combined reference, target, and background lights ($M_{\mu,\lambda}/L_{\mu,\lambda}$) for observer S2. First of two separate runs for this subject. The upper panel shows the HFP sensitivities determined on the spectral adapting fields, and the middle panel the sensitivities on the bichromatic adapting fields. The small open (white dots) and filled (black dots) circles plotted in the upper and middle panels, respectively, are best-fitting version of Equation 4. The corresponding residuals are plotted in the bottom panel. Other details as **Figure 4**.

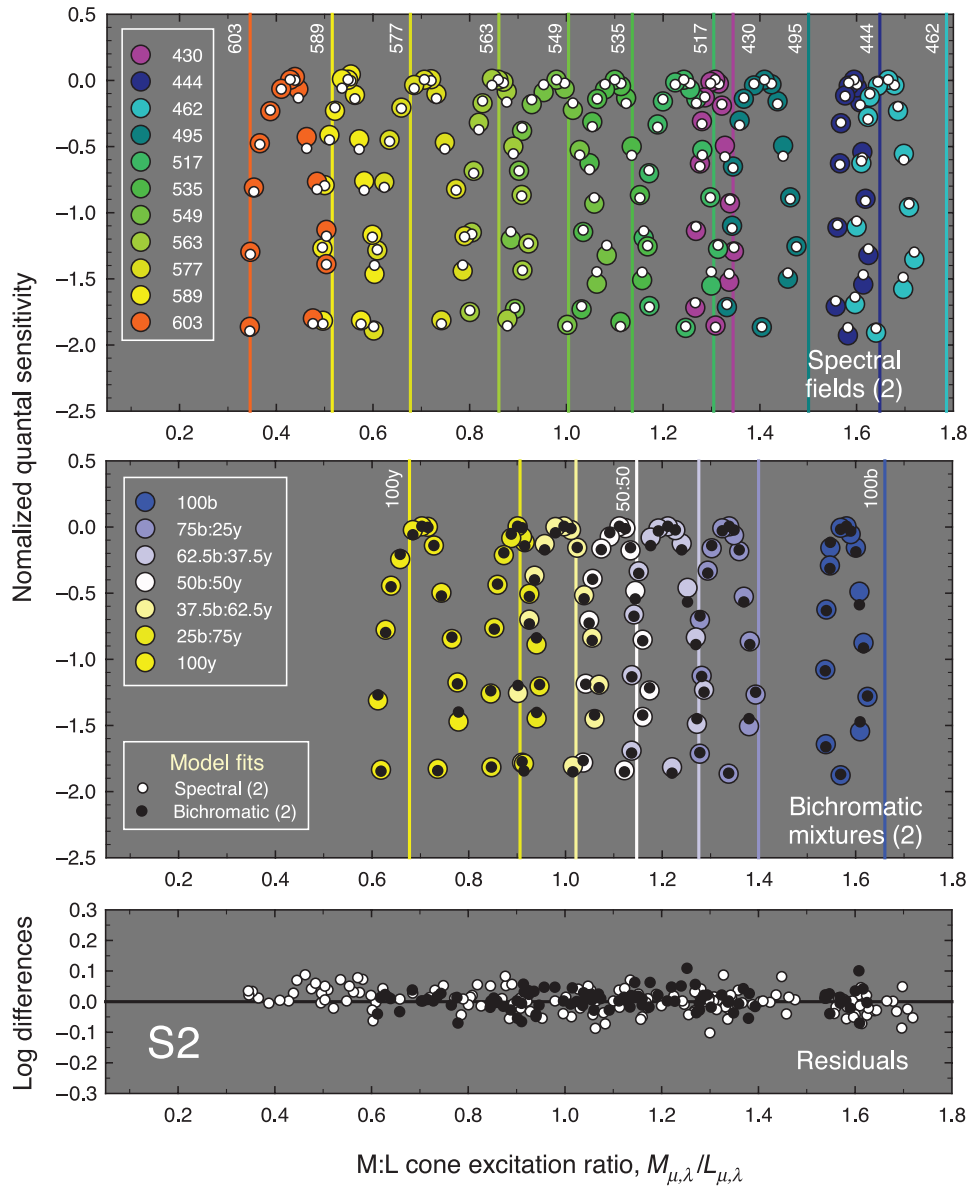


Figure A2. Luminous efficiencies (HFP matches) versus M:L-cone excitation ratios elicited by the combined reference, target, and background lights ($M_{\mu,\lambda}/L_{\mu,\lambda}$) for observer S2. Second of two separate runs. Other details as Figure 4.

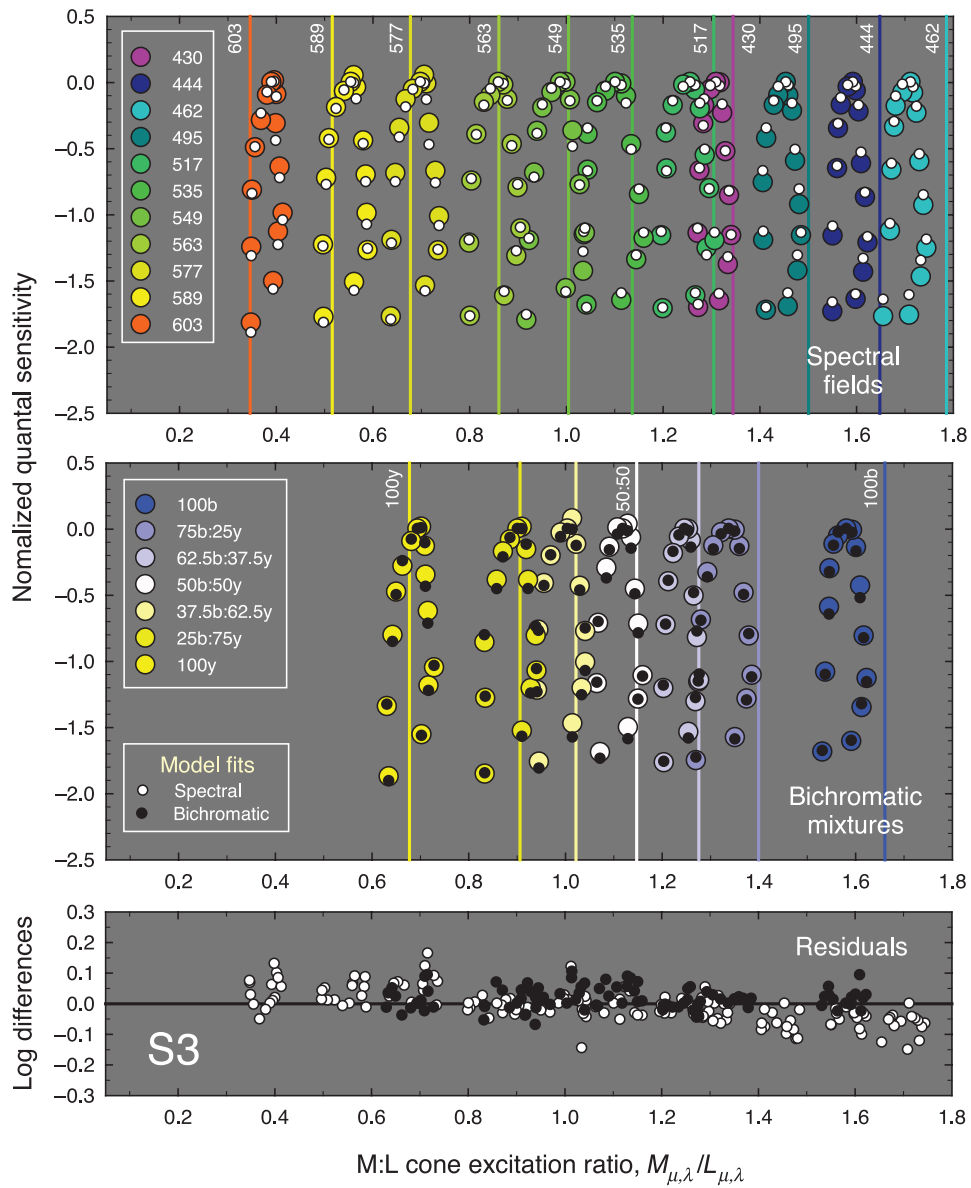


Figure A3. Luminous efficiencies (HFP matches) versus M:L-cone excitation ratios elicited by the combined reference, target, and background lights ($M_{\mu,\lambda}/L_{\mu,\lambda}$) for observer S3. Other details as Figure 4.

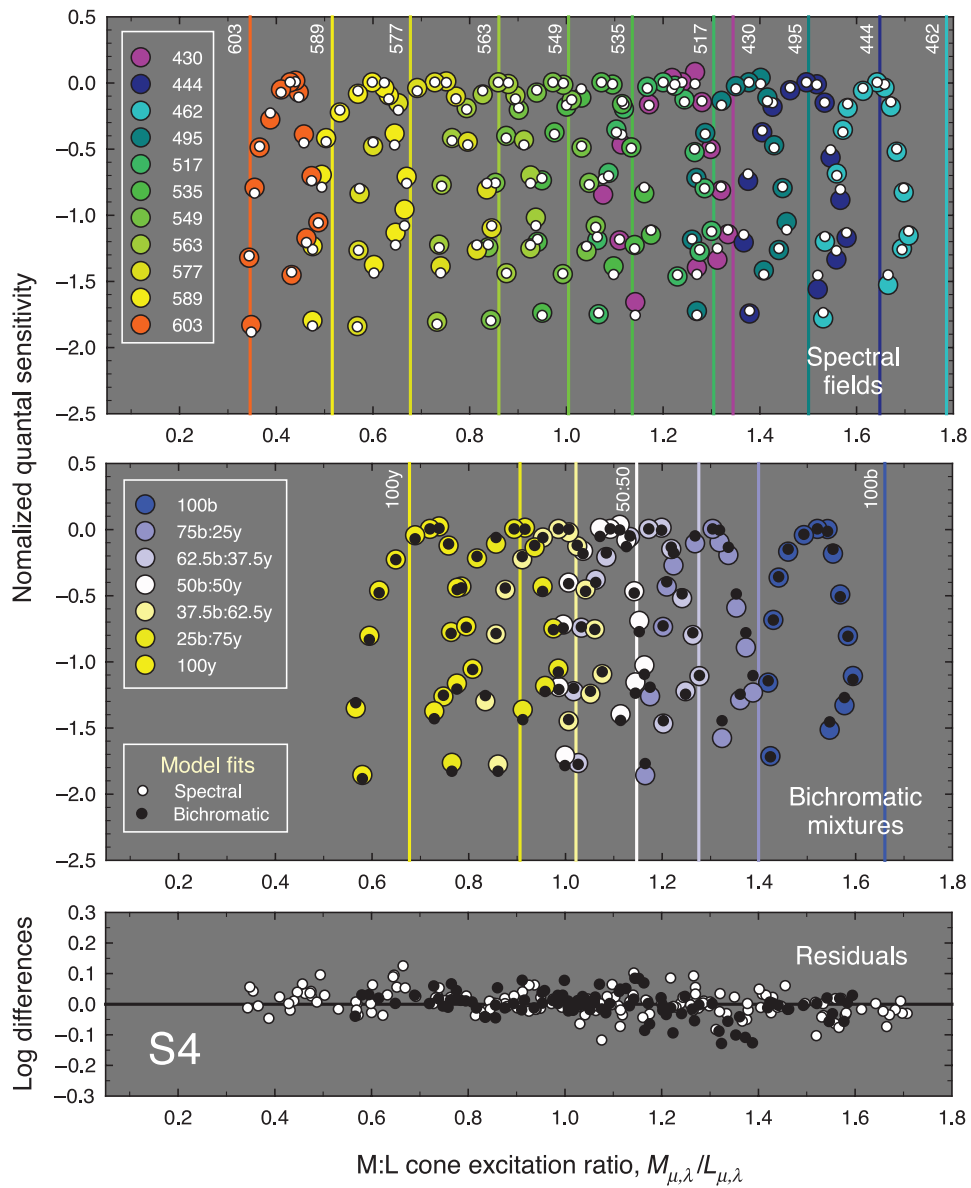


Figure A4. Luminous efficiencies (HFP matches) versus M:L-cone excitation ratios elicited by the combined reference, target, and background lights ($M_{\mu,\lambda}/L_{\mu,\lambda}$) for observer S4. Other details as Figure 4.

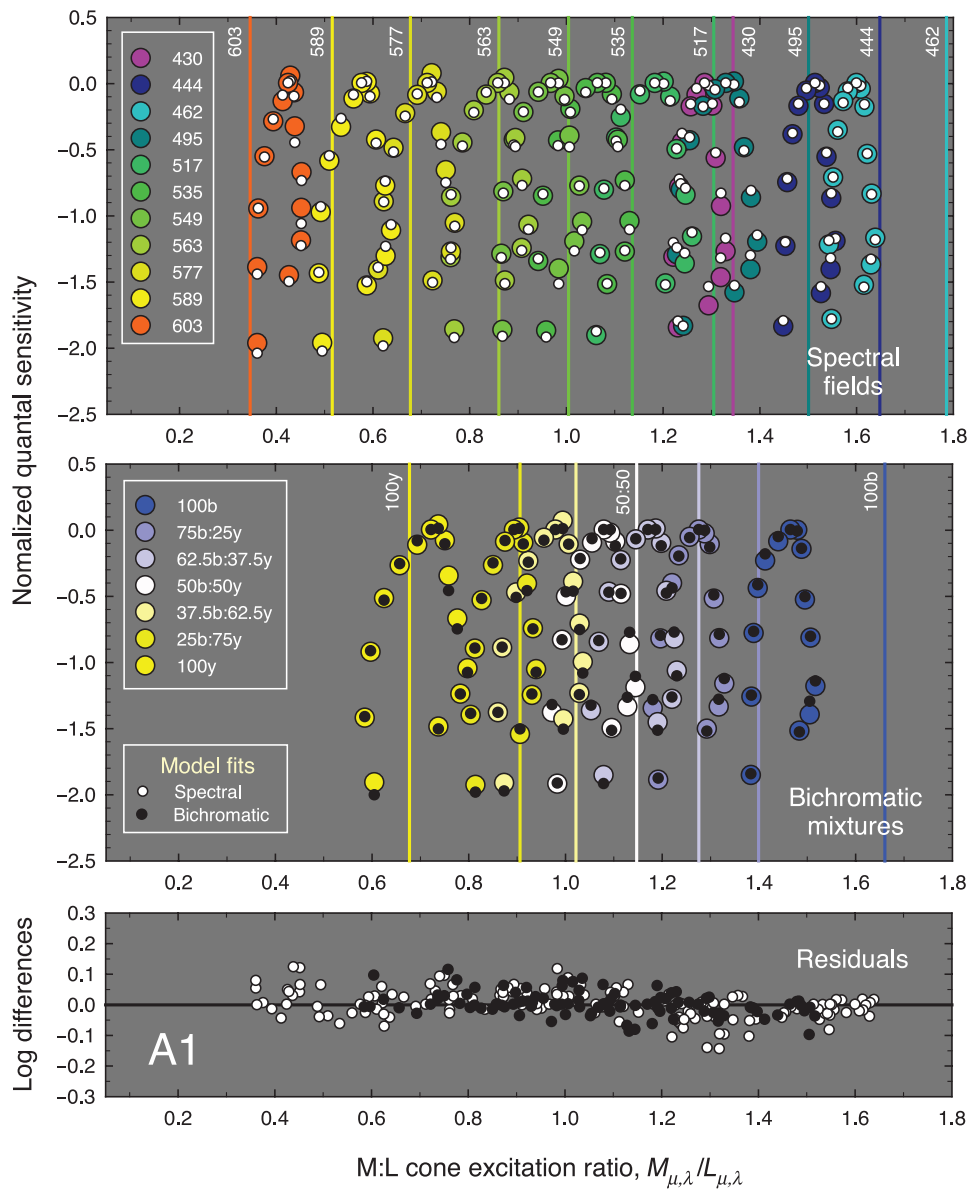


Figure A5. Luminous efficiencies (HFP sensitivities) versus M:L-cone excitation ratios ($M_{\mu,\lambda}/L_{\mu,\lambda}$) elicited by the combined reference, target, and background lights for observer A1. Other details as Figure 4.

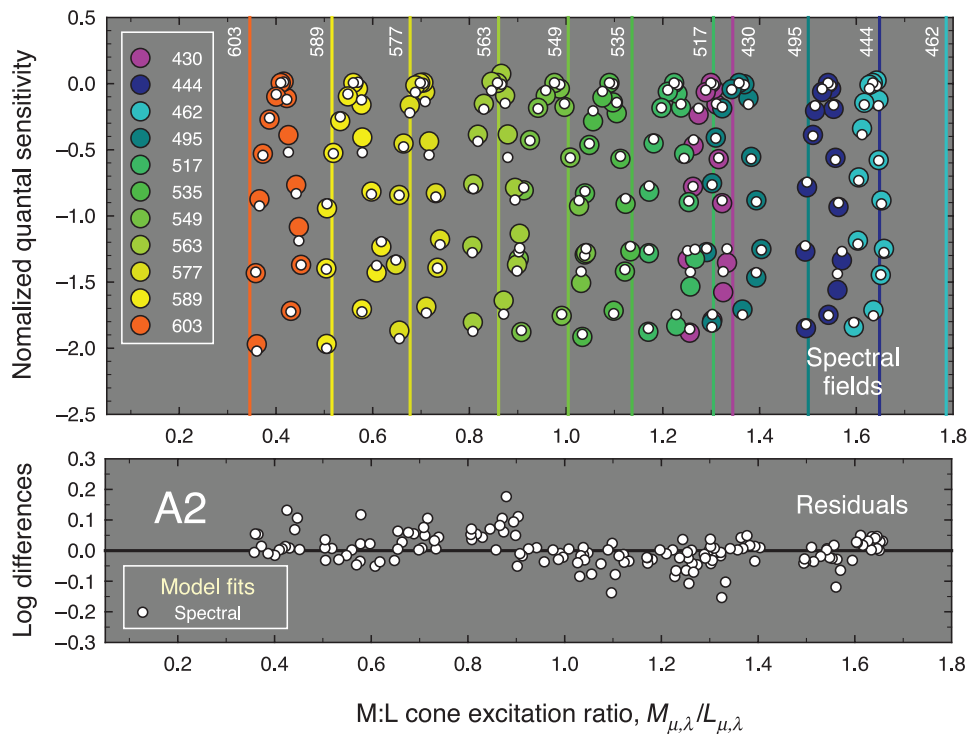


Figure A6. Luminous efficiencies (HFP sensitivities) versus M:L-cone excitation ratios ($M_{\mu,\lambda}/L_{\mu,\lambda}$) elicited by the combined reference, target, and background lights for observer A2. This subject made no measurements on bichromatic fields. Other details as Figure 4.

Acknowledgments

This work was supported by the Deutsche Forschungsgemeinschaft (Bonn) grants SFB 325 Tp A13 and Sh23/5-1 awarded to LTS, SFB 430 Tp A6 and JA997/5-1 awarded to HJ, and a Hermann- und Lilly-Schilling-Stiftung-Professur awarded to LTS, by a BBSRC and a Wellcome Trust grant awarded to AS, and by Fight for Sight. We thank Rhea Eskew for helpful and challenging discussions concerning the model and Bruce Henning for comments on the manuscript.

Commercial relationships: none.

Corresponding authors: Andrew Stockman, Herbert Jägle or Lindsay T. Sharpe.

Email: a.stockman@ucl.ac.uk, herbert.jaegle@uni-tuebingen.de or ltsharp@cvrl.org.

Address: Institute of Ophthalmology, 11-43 Bath Street, London, EC1V 9EL, UK.

References

- Adam, A. (1969). Foveal red–green ratios of normals, colorblinds and heterozygotes. *Proceedings of the Tel-Hashomer Hospital: Tel-Aviv*, 8, 2–6.
- Albrecht, J., Jägle, H., Hood, D. C., & Sharpe, L. T. (2002). The multifocal electroretinogram (mfERG)

and cone isolating stimuli: Variation in L- and M-cone driven signals across the retina. *Journal of Vision*, 2(8):2, 543–558, <http://journalofvision.org/2/8/2/>, doi:10.1167/2.8.2. [PubMed] [Article]

- Bieber, M. L., Kraft, J. M., & Werner, J. S. (1998). Effects of known variations in photopigments on L/M cone ratios estimated from luminous efficiency functions. *Vision Research*, 38, 1961–1966. [PubMed]
- Bone, R. A., Landrum, J. T., & Cains, A. (1992). Optical density spectra of the macular pigment *in vivo* and *in vitro*. *Vision Research*, 32, 105–110. [PubMed]
- Brainard, D. H., Roorda, A., Yamauchi, Y., Calderone, J. B., Metha, A., Neitz, M., et al. (2000). Functional consequences of the relative numbers of L and M cones. *Journal of the Optical Society of America A, Optics, Image Science, and Vision*, 17, 607–614. [PubMed]
- Carroll, J., McMahon, C., Neitz, M., & Neitz, J. (2000). Flicker-photometric electroretinogram estimates of L: M cone photoreceptor ratio in men with photopigment spectra derived from genetics. *Journal of the Optical Society of America A, Optics, Image Science, and Vision*, 17, 499–509. [PubMed]
- Carroll, J., Neitz, J., & Neitz, M. (2002). Estimates of L:M cone ratio from ERG flicker photometry and genetics. *Journal of Vision*, 2(8):1, 531–542, <http://journalofvision.org/2/8/1/>, doi:10.1167/2.8.1. [PubMed] [Article]

- Chaparro, A., Stromeyer, C. F., III, Kronauer, R. E., & Eskew, R. T., Jr. (1994). Separable red–green and luminance detectors for small flashes. *Vision Research*, *34*, 751–762. [[PubMed](#)]
- Conner, J. D., & MacLeod, D. I. (1977). Rod photoreceptors detect rapid flicker. *Science*, *195*, 689–699. [[PubMed](#)]
- Crone, R. A. (1959). Spectral sensitivity in color-defective subjects and heterozygous carriers. *American Journal of Ophthalmology*, *48*, 231–238. [[PubMed](#)]
- Deeb, S. S., Hayashi, T., Winderickx, J., & Yamaguchi, T. (2000). Molecular analysis of human red/green visual pigment gene locus: Relationship to color vision. In K. Palczewski (Ed.), *Vertebrate phototransduction and the visual cycle, Part B. Methods in enzymology* (vol. 316, pp. 651–670). New York: Academic Press.
- De Lange, H. (1958). Research into the dynamic nature of the human fovea–cortex systems with intermittent and modulated light. I. Attenuation characteristics with white and colored light. *Journal of the Optical Society of America*, *48*, 777–784. [[PubMed](#)]
- De Lange, H. (1961). Eye's response at flicker fusion to square-wave modulation of a test field surrounded by a large steady field of equal mean luminance. *Journal of the Optical Society of America*, *51*, 415–421.
- De Vries, H. (1946). Luminosity curves of trichromats. *Nature*, *157*, 736–737.
- De Vries, H. (1948a). The heredity of the relative numbers of red and green receptors in the human eye. *Genetica*, *24*, 199–212.
- De Vries, H. (1948b). The luminosity curve of the eye as determined by measurements with the flicker photometer. *Physica*, *14*, 319–348.
- Dobkins, K. R., Thiele, A., & Albright, T. D. (2000). Comparisons of red–green equiluminance points in humans and macaques: Evidence for different L:M cone ratios between species. *Journal of the Optical Society of America A, Optics, Image Science, and Vision*, *17*, 545–556. [[PubMed](#)]
- Drum, B. A. (1977). Cone interactions at high flicker frequencies: Evidence for cone latency differences? *Journal of the Optical Society of America*, *67*, 1601–1603.
- Eisner, A. (1982). Comparison of flicker-photometric and flicker-threshold spectral sensitivities while the eye is adapted to colored backgrounds. *Journal of the Optical Society of America*, *72*, 517–518. [[PubMed](#)]
- Eisner, A., & MacLeod, D. I. (1981). Flicker photometric study of chromatic adaptation: Selective suppression of cone inputs by colored backgrounds. *Journal of the Optical Society of America*, *71*, 705–717. [[PubMed](#)]
- Eskew, R. T., Jr., McLellan, J. S., & Giulianini, F. (1999). Chromatic detection and discrimination. In K. Gegenfurtner & L. T. Sharpe (Eds.), *Color vision: From genes to perception*. Cambridge: Cambridge University Press.
- Green, D. G. (1968). The contrast sensitivity of the colour mechanisms of the human eye. *The Journal of Physiology*, *196*, 415–429. [[PubMed](#)] [[Article](#)]
- Gunther, K. L., & Dobkins, K. R. (2002). Individual differences in chromatic (red/green) contrast sensitivity are constrained by the relative numbers of L- versus M-cones in the eye. *Vision Research*, *42*, 1367–1378. [[PubMed](#)]
- Hofer, H., Carroll, J., Neitz, J., Neitz, M., & Williams, D. R. (2005). Organization of the human trichromatic cone mosaic. *Journal of Neuroscience*, *25*, 9669–9679. [[PubMed](#)] [[Article](#)]
- Ikeda, M., & Urakubo, M. (1968). Flicker HRTF as test of color vision. *Journal of the Optical Society of America*, *58*, 27–31. [[PubMed](#)]
- Jacobs, G. H., Neitz, J., & Krogh, K. (1996). Electroretinogram flicker photometry and its applications. *Journal of the Optical Society of America A, Optics, Image Science, and Vision*, *13*, 641–648. [[PubMed](#)]
- Kelly, D. H. (1961). Visual responses to time-dependent stimuli. I. Amplitude sensitivity measurements. *Journal of the Optical Society of America*, *51*, 422–429. [[PubMed](#)]
- Kelly, D. H. (1974). Spatio-temporal frequency characteristics of color-vision mechanisms. *Journal of the Optical Society of America*, *64*, 983–990. [[PubMed](#)]
- King-Smith, P. E., & Webb, J. R. (1974). The use of photopic saturation in determining the fundamental spectral sensitivity curves. *Vision Research*, *14*, 421–429. [[PubMed](#)]
- Kremers, J., Scholl, H. P., Knau, H., Berendschot, T. T., & Sharpe, L. T. (2000). L/M-cone ratios in human trichromats assessed by psychophysics, electroretinography and retinal densitometry. *Journal of the Optical Society of America A, Optics, Image Science, and Vision*, *17*, 517–526. [[PubMed](#)]
- Lennie, P., Pokorny, J., & Smith, V. C. (1993). Luminance. *Journal of the Optical Society of America A, Optics and Image Science*, *10*, 1283–1293. [[PubMed](#)]
- Lutze, M., Cox, N. J., Smith, V. C., & Pokorny, J. (1990). Genetic studies of variation in Rayleigh and photometric matches in normal trichromats. *Vision Research*, *30*, 149–162. [[PubMed](#)]
- MacLeod, D. I. (1978). Visual sensitivity. *Annual Review of Psychology*, *29*, 613–645. [[PubMed](#)]
- Marks, L. E., & Bornstein, M. H. (1973). Spectral sensitivity by constant CFF: Effect of chromatic

- adaptation. *Journal of the Optical Society of America*, 63, 220–226. [PubMed]
- Matin, L. (1968). Critical duration, the differential luminance threshold, critical flicker frequency, and visual adaptation: A theoretical treatment. *Journal of the Optical Society of America*, 58, 404–415. [PubMed]
- Neitz, M., & Neitz, J. (1998). Molecular genetics and the biological basis of color vision. In W. G. K. Backhaus, R. Kliegl, & J. S. Werner (Eds.), *Color vision: Perspectives from different disciplines* (pp. 101–119). Berlin: Walter de Gruyter.
- Rushton, W. A., & Baker, H. D. (1964). Red/green sensitivity in normal vision. *Vision Research*, 4, 75–85. [PubMed]
- Sharpe, L. T., de Luca, E., Hansen, T., Jägle, H., & Gegenfurtner, K. R. (2006). Advantages and disadvantages of human dichromacy. *Journal of Vision*, 6(3):3, 213–223, <http://journalofvision.org/6/3/3/>, doi:10.1167/6.3.3. [PubMed] [Article]
- Sharpe, L. T., Stockman, A., Jagla, W., & Jägle, H. (2005). A luminous efficiency function, $V^*(\lambda)$, for daylight adaptation. *Journal of Vision*, 5(11):3, 948–968, <http://journalofvision.org/5/11/3/>, doi:10.1167/5.11.3. [PubMed] [Article]
- Sharpe, L. T., Stockman, A., Jägle, H., Knau, H., Klausen, G., Reitner, A., et al. (1998). Red, green, and red–green hybrid photopigments in the human retina: Correlations between deduced protein sequences and psychophysically-measured spectral sensitivities. *Journal of Neuroscience*, 18, 10053–10069. [PubMed] [Article]
- Sharpe, L. T., Stockman, A., Knau, H., & Jägle, H. (1998). Macular pigment densities derived from central and peripheral spectral sensitivity differences. *Vision Research*, 38, 3233–3239. [PubMed]
- Sharpe, L. T., Stockman, A., & MacLeod, D. I. (1989). Rod flicker perception: Scotopic duality, phase lags and destructive interference. *Vision Research*, 29, 1539–1559. [PubMed]
- Smith, V. C., & Pokorny, J. (1975). Spectral sensitivity of the foveal cone photopigments between 400 and 500 nm. *Vision Research*, 15, 161–171. [PubMed]
- Sperling, G., & Sondhi, M. M. (1968). Model for visual luminance discrimination and flicker detection. *Journal of the Optical Society of America*, 58, 1133–1145. [PubMed]
- Stiles, W. S. (1978). *Mechanisms of colour vision*. London: Academic.
- Stockman, A., Langendörfer, M., Smithson, H. E., & Sharpe, L. T. (2006). Human cone light adaptation: From behavioral measurements to molecular mechanisms. *Journal of Vision*, 6(11):5, 1194–1213, <http://journalofvision.org/6/11/5/>, doi:10.1167/6.11.5. [PubMed] [Article]
- Stockman, A., MacLeod, D. I., & DePriest, D. D. (1991). The temporal properties of the human short-wave photoreceptors and their associated pathways. *Vision Research*, 31, 189–208. [PubMed]
- Stockman, A., MacLeod, D. I., & Vivien, J. A. (1993). Isolation of the middle- and long-wavelength-sensitive cones in normal trichromats. *Journal of the Optical Society of America A, Optics, Image Science, and Vision*, 10, 2471–2490. [PubMed]
- Stockman, A., Montag, E. D., & MacLeod, D. I. A. (1991). Large changes in phase delay on intense bleaching backgrounds. *Investigative Ophthalmology & Visual Science*, 32, 841.
- Stockman, A., Montag, E. D., & Plummer, D. J. (2006). Paradoxical shifts in human colour sensitivity caused by constructive and destructive interference between signals from the same cone class. *Visual Neuroscience*, 23, 471–478. [PubMed]
- Stockman, A., & Plummer, D. J. (1994). The luminance channel can be opponent? *Investigative Ophthalmology & Visual Science*, 35, 1572.
- Stockman, A., & Plummer, D. J. (2005a). Long-wavelength adaptation reveals slow, spectrally-opponent inputs to the human luminance pathway. *Journal of Vision*, 5(9):5, 702–716, <http://journalofvision.org/5/9/5/>, doi:10.1167/5.9.5. [PubMed] [Article]
- Stockman, A., & Plummer, D. J. (2005b). Spectrally-opponent inputs to the human luminance pathway: Slow +L and –M cone inputs revealed by low to moderate long-wavelength adaptation. *The Journal of Physiology*, 566, 77–91. [PubMed] [Article]
- Stockman, A., Plummer, D. J., & Montag, E. D. (2005). Spectrally-opponent inputs to the human luminance pathway: Slow +M and –L cone inputs revealed by intense long-wavelength adaptation. *The Journal of Physiology*, 566, 61–76. [PubMed] [Article]
- Stockman, A., & Sharpe, L. T. (2000). Spectral sensitivities of the middle- and long-wavelength sensitive cones derived from measurements in observers of known genotype. *Vision Research*, 40, 1711–1737. [PubMed]
- Stockman, A., Sharpe, L. T., & Fach, C. (1999). The spectral sensitivity of the human short-wavelength cones derived from thresholds and color matches. *Vision Research*, 39, 2901–2927. [PubMed]
- Stromeyer, C. F., III, Chaparro, A., Tolia, A. S., & Kronauer, R. E. (1997). Colour adaptation modifies the long-wave versus middle-wave cone weights and temporal phases in human luminance (but not red–green) mechanism. *The Journal of Physiology*, 499, 227–254. [PubMed] [Article]
- Stromeyer, C. F., III, Cole, G. R., & Kronauer, R. E. (1987). Chromatic suppression of cone inputs to the

- luminance flicker mechanisms. *Vision Research*, 27, 1113–1137. [[PubMed](#)]
- Stromeyer, C. F., III, Gowdy, P. D., Chaparro, A., Kladakis, S., Willen, J. D., & Kronauer, R. E. (2000). Colour adaptation modifies the temporal properties of the long- and middle-wave cone signals in the human luminance mechanism. *The Journal of Physiology*, 526, 177–194. [[PubMed](#)] [[Article](#)]
- Swanson, W. H. (1993). Chromatic adaptation alters spectral sensitivity at high temporal frequencies. *Journal of the Optical Society of America A, Optics and Image Science*, 10, 1294–1303. [[PubMed](#)]
- Swanson, W. H., Pokorny, J., & Smith, V. C. (1987). Effects of temporal frequency on phase-dependent sensitivity to heterochromatic flicker. *Journal of the Optical Society of America A, Optics and Image Science*, 4, 2266–2273. [[PubMed](#)]
- Tranchina, D., Gordon, J., & Shapley, R. M. (1984). Retinal light adaptation—Evidence for a feedback mechanism. *Nature*, 310, 314–316. [[PubMed](#)]
- Norren, D., & Vos, J. J. (1974). Spectral transmission of the human ocular media. *Vision Research*, 14, 1237–1244. [[PubMed](#)]
- Vimal, R. L., Pokorny, J., Smith, V. C., & Shevell, S. K. (1989). Foveal cone thresholds. *Vision Research*, 29, 61–78. [[PubMed](#)]
- Vos, J. J., & Walraven, P. L. (1971). On the derivation of the foveal receptor primaries. *Vision Research*, 11, 799–818. [[PubMed](#)]
- Watson, A. B. (1986). Temporal sensitivity. In K. Boff, L. Kaufman, & J. Thomas (Eds.), *Handbook of perception and human performance* (vol. 1, pp. 6–1–6–43). New York: Wiley.
- Wesner, M. F., Pokorny, J., Shevell, S. K., & Smith, V. C. (1991). Foveal cone detection statistics in color-normals and dichromats. *Vision Research*, 31, 1021–1037. [[PubMed](#)]
- Winderickx, J., Battisti, L., Hibiya, Y., Motulsky, A. G., & Deeb, S. S. (1993). Haplotype diversity in the human red and green opsin genes: Evidence for frequent sequence exchange in exon 3. *Human Molecular Genetics*, 2, 1413–1421. [[PubMed](#)]